Gaussian Regression-Driven Tensorized Incomplete Multi-View Clustering with Dual Manifold Regularization

Zhenhao Zhong[1] **Zhibin Gu**[1*] **Pengpeng Yang**[2] **Yaqian Zhou**[1] **Ruiqiang Guo**[1]
[1]College of Computer and Cyber Security, Hebei Normal University, China
[2]College of computer and Information Technology, China Three Gorges University, China
guzhibin@hebtu.edu.cn

Abstract

Tensorized Incomplete Multi-View Clustering (TIMVC) algorithms have attracted growing attention for their ability to capture high-order correlations across multiple views. However, most existing TIMVC methods rely on simplistic noise assumptions using specific norms (e.g., ℓ_1 or $\ell_{2,1}$), which fail to reflect the complex noise patterns encountered in real-world scenarios. Moreover, they primarily focus on modeling the global Euclidean structure of the tensor representation, while overlooking the preservation of local manifold structures. To address these limitations, we propose a novel approach, **G**a**U**ssian regress**I**on-driven **T**IMVC with dual m**A**nifold **R**egularization (**GUITAR**). Specifically, we employ a Gaussian regression model to characterize complex noise distributions in a more realistic and flexible manner. Meanwhile, a dual manifold regularization is introduced in tensor representation learning, simultaneously modeling manifold information at both the view-specific and cross-view consensus levels, thereby promoting intra-view and inter-view consistency in the tensor representation. Furthermore, to better capture the intrinsic low-rank structure, we propose the high-preservation ℓ_δ-norm tensor rank constraint, which applies differentiated penalties to the singular values, thereby enhancing the robustness of the tensor representation. In addition, an efficient optimization algorithm is developed to solve the resulting non-convex problem with provable convergence. Extensive experiments on six datasets demonstrate that our method outperforms SOTA approaches. The code is available at `https://github.com/RockfireTip/GUITAR`.

1 Introduction

With the rapid expansion of multi-view data across a wide range of domains, multi-view clustering (MVC) has emerged as a key unsupervised learning paradigm for integrating heterogeneous information [1–5]. By exploiting the complementarity and consistency among multiple views, MVC can significantly enhance clustering performance. However, real-world datasets often suffer from partially missing views due to sensor failures, privacy concerns, or data corruption. Such incompleteness hinders the accurate modeling of inter-view relationships, thereby limiting the effectiveness of conventional MVC methods in assigning data points to their correct clusters. As a result, incomplete multi-view clustering (IMVC) has garnered growing attention for its potential to exploit incomplete multi-view data and uncover their underlying structure [6–8].

Incomplete multi-view clustering (IMVC) aims to uncover correlations across multiple views in the presence of missing data by employing various strategies, thereby enabling more accurate data

*Corresponding author

39th Conference on Neural Information Processing Systems (NeurIPS 2025).

clustering. For example, Wen et al. [9] developed a confidence-based neighborhood consensus graph model, which leverages the nearest-neighbor assumption to effectively extract group structure information. Wang et al. [10] integrated missing data imputation with bipartite graph learning in a unified framework, leading to improved clustering accuracy and efficiency. Furthermore, Liu et al. [11] proposed a joint optimization framework for kernel matrix completion and multi-kernel alignment, enabling collaborative kernel and clustering optimization through alternating iterations. However, the methods mentioned above primarily focus on capturing linear correlations between views, neglecting the modeling of higher-order relationships, which limits clustering performance. To address this limitation, recent tensor-based approaches have been proposed to effectively capture higher-order correlations in multi-view data [12–14]. For instance, Wen et al.[12] proposed a unified framework that seamlessly integrates missing-view inference with low-rank tensor learning, enabling joint recovery of latent information in missing views and modeling of high-order inter-view correlations. Zhang et al. [15] reformulated IMVC as a joint learning problem of incomplete similarity graphs and complete tensor representation, effectively capturing inter-view correlations and suppressing noise via structured tensor decomposition. In addition, EDISON [14] leverages an enhanced dictionary representation to infer missing data and build anchor graphs, enhancing robustness against data incompleteness.

Despite the impressive clustering performance achieved by TIMVC methods through exploiting high-order correlations across views, there remain three limitations that warrant further improvement. First, most existing TIMVC approaches rely on specific norms (e.g., ℓ_1 or $\ell_{2,1}$) to model noise, which implicitly assumes that the noise follows a predefined distribution. However, in real-world applications, noise often exhibits more complex characteristics, making it difficult for a single norm to accurately capture its nature, thus leading to suboptimal tensor representations. Second, the majority of TIMVC methods focus primarily on modeling the global Euclidean structure of the tensor representation, while neglecting the preservation of local manifold structures, which are often crucial for clustering tasks. Third, the commonly adopted Tensor Nuclear Norm (TNN) serves as a surrogate for tensor rank but is known to be a biased estimator, which may result in suboptimal tensor recovery and limit the model's overall effectiveness.

To address the aforementioned challenges, we introduce a novel model, Gaussian regression-driven tensorized incomplete multiview clustering with dual manifold regularization (GUITAR). Specifically, first, GUITAR utilizes Gaussian regression to model noise as a Gaussian distribution, facilitating a more effective adaptation to diverse noise types and resulting in a more discriminative affinity matrix that better captures the true structure of the data. Second, we propose a dual Laplacian manifold regularization approach, which enables both the view-specific local manifold structures and the cross-view consensus manifold structure to jointly enhance the representational capacity of the affinity matrix. Additionally, we design a novel tensor rank regularization function that adaptively applies varying degrees of penalty to singular values of the tensor, allowing for the modeling of prior structural knowledge inherent in the tensor data. Figure 1 illustrates the framework of GUITAR. Compared to existing TIMVC methods, the contributions of this work can be summarized as follows:

- We propose a novel tensorized incomplete multi-view clustering framework that incorporates a Gaussian regression-based noise modeling strategy to adapt to diverse real-world noise distributions, enabling more discriminative affinity matrices and more accurate tensor representations.
- A dual manifold regularization framework is introduced, which preserves local geometric structures within individual views while capturing cross-view consensus structures, thereby improving the affinity matrix's capacity to model inter-sample relationships.
- To better capture intrinsic low-rank structures, we introduce an adaptive tensor rank constraint that imposes differentiated penalties on singular values, thereby enhancing the robustness of tensor representations.
- An efficient ADMM-based solver is developed with theoretical convergence guarantees. Extensive experiments demonstrate the superiority of our approach.

2 Related work

Incomplete Multi-view Clustering (IMVC) methods can be broadly categorized into matrix-based and tensor-based approaches, depending on whether they leverage high-order correlations across multiple views.

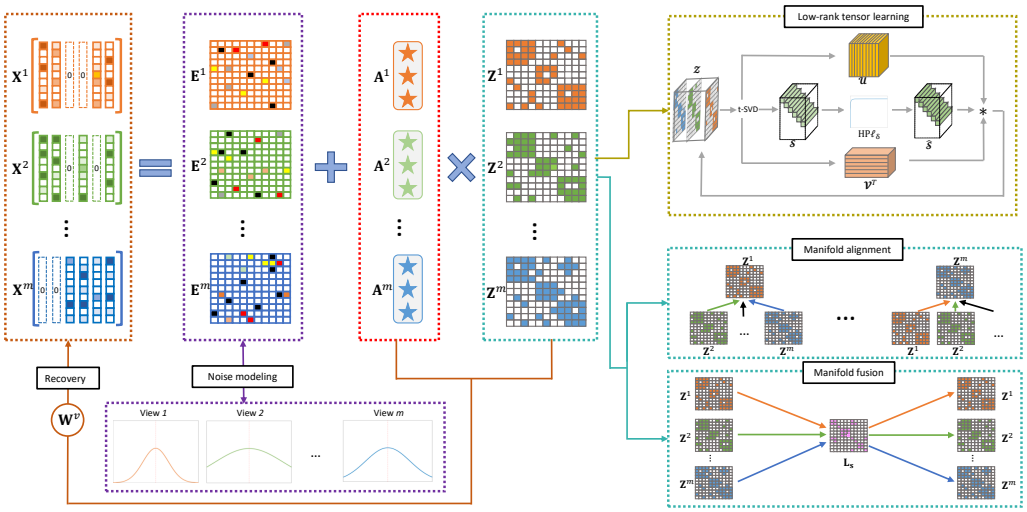

Figure 1: The proposed model consists of four main components: noise modeling, low-rank tensor learning, manifold alignment, and manifold fusion. Noise modeling captures complex noise caused by reconstruction errors and missing data. Low-rank tensor learning preserves essential structural information by imposing a robust low-rank constraint. Manifold alignment and manifold fusion collaboratively align and integrate manifold structures across multiple views.

Matrix-based methods typically impose structural constraints or optimization strategies on feature or similarity matrices to integrate multi-view information. For instance, the DAIMC model [16] proposes a weighted semi-non-negative matrix factorization framework that incorporates l_{21}-norm regularization to reduce the impact of missing views. Yu et al. [17] propose constructing prototype-sample affinity matrices and cross-view prototypes to jointly unify representation learning and clustering under incomplete data. Recent deep learning-based matrix constraint methods have further advanced this area. Lin et al. [18] unify multi-view consistency learning and missing view recovery, maximizing mutual information through contrastive learning while minimizing conditional entropy to aid view completion. Tang and Liu [7] develop a dual optimization framework to dynamically interpolate missing views and select interpolated samples for training, thus reducing the impact of semantically inconsistent interpolations on clustering performance.

Tensor-based methods impose low-rank structural constraints on the three-dimensional tensor reconstructed from incomplete multi-view data, leveraging cross-view high-order information to facilitate the completion of missing data [15, 19, 20]. Zhang et al. [15] decompose the tensor into a sparse tensor for noise modeling and a low-rank intrinsic tensor for capturing true similarities, enhancing the discriminative power of the similarity matrix. Wu et al. [13] propose the use of kernel tensors to model inter-view correlations and impose low-rank constraints to enhance cross-view consistency, facilitating effective completion of missing kernel entries. Huang et al. [20] employ tensor decomposition to jointly perform missing value imputation and feature selection, effectively capturing shared structures across multiple views.

3 Proposed method

3.1 The GUITAR model

Given a multi-view dataset $\{\mathbf{X}^v\}_{v=1}^m$ consisting of m views and n samples, where $\mathbf{X}^v \in \mathbb{R}^{d_v \times n}$ denotes the feature matrix of the v-th view with d_v dimension, we build our method upon a tensor-based multi-view clustering framework [1, 21, 22], which can be generally formulated as follows:

$$\begin{aligned} &\min_{\{\mathbf{E}^v,\mathbf{Z}^v\}_{v=1}^m} \mathcal{R}(\boldsymbol{\mathcal{Z}}) + \alpha\mathcal{P}(\mathbf{E}^v) + \beta\mathcal{T}(\mathbf{Z}^v) \\ &\text{s.t. } \forall v,\ \mathbf{X}^v = \mathbf{X}^v\mathbf{Z}^v + \mathbf{E}^v, \boldsymbol{\mathcal{Z}} = \Phi(\mathbf{Z}^1, \mathbf{Z}^2, \ldots, \mathbf{Z}^m), \end{aligned} \tag{1}$$

where α and β are trade-off parameters. $\mathbf{Z}^v \in \mathbb{R}^{n\times n}$ denotes the coefficient matrix of the v-th view, and $\mathbf{E}^v \in \mathbb{R}^{d_v\times n}$ represents the reconstruction error of the v-th view. The operator Φ stacks $\{\mathbf{Z}^v\}_{v=1}^m$ into a third-order tensor $\boldsymbol{\mathcal{Z}}$ whose rank is approximated by $\mathcal{R}(\cdot)$. $\mathcal{P}(\cdot)$ and $\mathcal{T}(\cdot)$ are used to model the reconstruction error and regularize the coefficient matrices, respectively.

Model (1) is capable of capturing high-order correlations across multiple views. However, it has been shown that selecting all sample points to construct the dictionary is unnecessary and leads to increased computational cost. In contrast, selecting a subset of t representative samples—referred to as anchors—is sufficient to form an expressive dictionary, and these anchors can be learned adaptively during optimization [23–25]. In this setting, the sample data $\mathbf{X}^v$ for each view v can be approximately reconstructed using an anchor matrix $\mathbf{A}^v \in \mathbb{R}^{d_v\times t}$ and a coefficient matrix $\mathbf{Z}^v \in \mathbb{R}^{t\times n}$, i.e., $\mathbf{X}^v \approx \mathbf{A}^v\mathbf{Z}^v$. Furthermore, to address the common issue of missing data in multi-view settings, we introduce a diagonal indicator matrix $\mathbf{W}^v \in \mathbb{R}^{n\times n}$ to encode sample availability in the v-th view. Specifically, the i-th diagonal entry of $\mathbf{W}^v$ is set to 1 if the i-th sample is missing in view v, and 0 otherwise. Under this formulation, the missing data can be estimated via the reconstruction $\mathbf{X}^v = \mathbf{A}^v\mathbf{Z}^v\mathbf{W}^v$ in the optimization process, which selectively reconstructs only the missing entries. Accordingly, Model (1) can be naturally extended to a tensorized and anchor-based formulation that accommodates incomplete multi-view data. The resulting model is defined as:

$$\begin{aligned}&\min_{\{\mathbf{E}^v,\mathbf{Z}^v,\mathbf{A}^v\}_{v=1}^m} \mathcal{R}(\boldsymbol{\mathcal{Z}}) + \alpha\mathcal{P}(\mathbf{E}^v) + \beta\,\mathcal{T}(\mathbf{Z}^v)\\ &\text{s.t. } \forall v,\ \mathbf{X}^v = \mathbf{A}^v\mathbf{Z}^v + \mathbf{E}^v, \boldsymbol{\mathcal{Z}} = \Phi(\mathbf{Z}^1,\mathbf{Z}^2,\ldots,\mathbf{Z}^m), (\mathbf{A}^v)^\top\mathbf{A}^v = \mathbf{I}\end{aligned} \tag{2}$$

$\mathbf{A}^v \in \mathbb{R}^{d_v\times t}$ denotes the anchor matrix for view v, where each column represents an anchor point. The orthogonality constraint $(\mathbf{A}^v)^\top\mathbf{A}^v = \mathbf{I}$ is commonly adopted in anchor-based multi-view clustering to enhance the discriminability and representativeness of the anchor points, thereby improving the clustering performance. The fundamental challenge in Model (2) lies in the principled design of regularization terms—$\mathcal{P}(\boldsymbol{\mathcal{Z}})$, $\mathcal{R}(\mathbf{E}^v)$, and $\mathcal{T}(\mathbf{Z}^v)$—to fully harness the complementary and heterogeneous information across multiple views for improved clustering performance. Although existing methods have proposed various constraints on the tensor representation $\boldsymbol{\mathcal{Z}}$, the error term $\mathbf{E}^v$, and their affinity matrix $\mathbf{Z}^v$, they often suffer from inherent limitations in expressiveness, flexibility, or robustness, particularly when dealing with complex, noisy, or incomplete multi-view data.

Limitation 1: inaccuracy in reconstruction error modeling. Common reconstruction error models, such as the ℓ_1 norm, $\ell_{2,1}$ norm, and Frobenius norm, each address specific types of noise-random, sample-specific, and Gaussian noise, respectively [26]. However, these approaches have key limitations. They fail to explicitly model noise distributions, and while the Frobenius norm assumes Gaussian noise for $\mathbf{E}^v$, it does so imprecisely, potentially introducing bias. Furthermore, in the case of incomplete views, missing data makes reconstruction errors more complex, a challenge these norms cannot adequately handle. To better model reconstruction error and handle complex noise, we introduce the Gaussian Regression Norm in tensor representation learning, which draws inspiration from the work of [27].

Definition 1 (Gaussian Regression Norm) *Consider the set of noise matrices $\{\mathbf{E}^v\}_{v=1}^m$. We assume that the noise within each view is independently and identically distributed (i.i.d.), with each noise vector following a multivariate Gaussian distribution $\mathcal{N}(\mathbf{e}_q^v \mid \boldsymbol{\mu}^v, \boldsymbol{\Sigma}^v)$. The Gaussian Regression Norm (GRN) is defined as:*

$$\|\{\mathbf{E}^v\}_{v=1}^m\|_{\mathrm{GRN}} = -\sum_{v=1}^{m}\left(\sum_{q=1}^{n}\ln\left(\mathcal{N}(\mathbf{e}_q^v \mid \boldsymbol{\mu}^v, \boldsymbol{\Sigma}^v)\right)\right) \tag{3}$$

where $\mathbf{e}_q^v \in \mathbb{R}^{d_v}$ denotes the noise vector corresponding to the q-th sample in the v-th view, $\boldsymbol{\mu}^v \in \mathbb{R}^{d_v}$ is the mean vector of the noise distribution, and $\boldsymbol{\Sigma}^v \in \mathbb{R}^{d_v\times d_v}$ is the view-specific covariance matrix.

The GRN represents the negative log-likelihood of observing the residual noise under a multivariate Gaussian model. Minimizing this norm encourages the residuals to follow the assumed distribution, allowing for adaptive modeling of intra-view noise characteristics, including correlation structure and scale. The detailed procedure for constructing $\|\{\mathbf{E}^v\}_{v=1}^m\|_{\mathrm{GRN}}$ is provided in Appendix A.1.

Limitation 2: inadequate utilization of manifold information. For the term $\mathcal{T}(\cdot)$, a commonly used constraint is the Laplacian manifold regularization, such as [28–30]. However, these methods

typically construct the Laplacian matrix solely based on a consensus similarity matrix, thereby neglecting manifold alignment across different view pairs. This oversight introduces bias into the consensus manifold constraint and compromises its effectiveness. To address this issue, we propose a novel constraint—Dual Manifold Regularization—designed to precisely capture the intrinsic structure of the data.

Definition 2 (Dual Manifold Regularization) *Given a set of coefficient matrices $\{\mathbf{Z}^v\}_{v=1}^m$, we define its Dual Manifold Regularization (DMR) term as follows:*

$$\|\{\mathbf{Z}^v\}_{v=1}^m\|_{\mathrm{DMR}} = \gamma \sum_{v=1}^{m} \sum_{\substack{v'=1 \\ v' \neq v}}^{m} \mathrm{Tr}\left(\mathbf{Z}^v \mathbf{L}^{v'} (\mathbf{Z}^v)^\top\right) + \sum_{v=1}^{m} \mathrm{Tr}\left(\mathbf{Z}^v \mathbf{L}_{\mathbf{s}} (\mathbf{Z}^v)^\top\right) \tag{4}$$

where $\mathrm{Tr}(\cdot)$ denotes the matrix trace operator, and $\mathbf{L}^v$ and $\mathbf{L}_{\mathbf{s}}$ represent the normalized Laplacian matrices for the v-th view and the consensus across all views, respectively. γ is the balancing parameter. The first term in the DMR encourages mutual constraints among the manifolds of each view, thereby enhancing their consistency. The second term constructs a consensus Laplacian matrix that fuses the manifolds across all views, capturing a unified manifold structure.

For each view v, the similarity $\mathbf{S}^v \in \mathbb{R}^{n \times n}$ is computed as $\mathbf{S}_{ij}^v = \frac{(\mathbf{z}_i^v)^\top \mathbf{z}_j^v}{\|\mathbf{z}_i^v\|_2 \|\mathbf{z}_j^v\|_2}$, where $\mathbf{z}_i^v \in \mathbb{R}^{d_v}$ denotes the feature vector of the i-th sample in view v. Each $\mathbf{S}^v$ is sparsified by retaining only the K-nearest neighbors. To integrate manifold information from multiple views, a consensus Laplacian $\mathbf{L}_{\mathbf{s}}$ is constructed based on the averaged similarity $\mathbf{S} = \frac{1}{m}\sum_{v=1}^m \mathbf{S}^v$, with the corresponding degree matrix $\mathbf{D}$. The normalized shared Laplacian is given by $\mathbf{L}_{\mathbf{s}} = \mathbf{I} - \mathbf{D}^{-1/2}\mathbf{S}\mathbf{D}^{-1/2}$. This construction provides a unified representation of manifold structures across all views. In the ideal case, the coefficient matrices $\mathbf{Z}^v$ from all views are expected to share a similar intrinsic structure of the data manifold. To this end, the consensus Laplacian matrix serves as a regularizer that promotes unified manifold learning across views. As illustrated in the construction of the consensus Laplacian matrix, it leverages a consensus similarity matrix to regularize a fused manifold across multiple views, thereby enhancing the clustering performance. A thorough elaboration of the Dual Manifold Regularization (DMR) term is contained within Appendix A.2.

Limitation 3: insufficient exploration of tensor prior information. Small singular values in tensor data typically correspond to noise, while large singular values capture the primary information. Traditional tensor rank approximation methods, such as the tensor nuclear norm [31] fail to differentiate between these two aspects. In contrast, non-convex approximations, such as the Logdet function[32, 33], the Laplace function[34, 35], and the ℓ_δ-norm [36] impose heavier penalties on small singular values and lighter penalties on larger ones, effectively removing noise while preserving critical information. Among these methods, the ℓ_δ-norm offers a compact approximation of tensor rank; however, it tends to impose stronger penalties on larger singular values compared to other non-convex approximations, potentially leading to the loss of important components. To address this issue, we propose an improved version of the ℓ_δ-norm , termed the High-Preservation ℓ_δ-norm, which better balances noise removal and the retention of useful information under the low-rank constraint. The formal definitions of the three components are as follows:

Definition 3 (High-Preservation ℓ_δ-norm) *Given a third-order tensor $\boldsymbol{\mathcal{Z}} \in \mathbb{R}^{n_1 \times n_2 \times n_3}$, the High-Preservation ℓ_δ-norm (HPℓ_δ) of $\boldsymbol{\mathcal{Z}}$ is defined as:*

$$\|\boldsymbol{\mathcal{Z}}\|_{\mathrm{HP}\ell_\delta} = \frac{1}{n_3}\sum_{k=1}^{n_3} \|\boldsymbol{\mathcal{Z}}_f^k\|_{\mathrm{HP}\ell_\delta} = \frac{1}{n_3}\sum_{k=1}^{n_3}\sum_{i=1}^{h} \frac{(1+\delta)\tanh\left(\boldsymbol{\mathcal{S}}_f^k(i,i)\right)}{\delta + \tanh\left(\boldsymbol{\mathcal{S}}_f^k(i,i)\right)} \tag{5}$$

where $h = \min(n_1, n_2)$ and δ is a positive scalar that controls the flexibility of the norm. Here, $\boldsymbol{\mathcal{S}}_f^k$ denotes the k-th frontal slice of the tensor $\boldsymbol{\mathcal{S}}_f$, which is obtained through the tensor singular value decomposition (t-SVD [37]) of $\boldsymbol{\mathcal{Z}}$'s k-th frontal slice $\boldsymbol{\mathcal{Z}}_f^k = \boldsymbol{\mathcal{U}}_f^k \boldsymbol{\mathcal{S}}_f^k (\boldsymbol{\mathcal{V}}_f^k)^\top$. A full exposition of $\mathrm{HP}\ell_\delta$ is presented in Appendix A.3.

Overall objective function of GUITAR: Building upon (2)-(5), the overall objective function of the GUITAR model is as follows:

$$\begin{aligned}\min_{\{\mathbf{E}^v,\mathbf{Z}^v,\mathbf{A}^v\}_{v=1}^m,\boldsymbol{\mathcal{Z}}} &\|\boldsymbol{\mathcal{Z}}\|_{\mathrm{HP}\ell_\delta}+\lambda_1\|\{\mathbf{E}^v\}_{v=1}^m\|_{\mathrm{GRN}}+\lambda_2\|\{\mathbf{Z}^v\}_{v=1}^m\|_{\text{DMR-1}}+\lambda_3\|\{\mathbf{Z}^v\}_{v=1}^m\|_{\text{DMR-2}}\\ &\text{s.t. } \forall v,\mathbf{X}^v=\mathbf{A}^v\mathbf{Z}^v+\mathbf{E}^v,\boldsymbol{\mathcal{Z}}=\Phi(\mathbf{Z}^1,\mathbf{Z}^2,\ldots,\mathbf{Z}^m),(\mathbf{A}^v)^\top\mathbf{A}^v=\mathbf{I}\end{aligned} \tag{6}$$

where the parameter $\boldsymbol{\mu}^v$ in the GRN term is set to a zero vector to simplify the optimization process. The term $\|\boldsymbol{\mathcal{Z}}\|_{\mathrm{HP}\ell_\delta}$ imposes a low-rank constraint on the tensor $\boldsymbol{\mathcal{Z}}$. The employed HPℓ_δ norm is a variant of the standard ℓ_δ norm. It penalizes small singular values similarly to the ℓ_δ norm, while applying relatively milder penalties to larger singular values. This design helps to preserve more critical structural information in the data. $\|\{\mathbf{E}^v\}_{v=1}^m\|_{\mathrm{GRN}}$ introduces a novel formulation for the reconstruction error model. Compared to traditional norms such as the ℓ_1 norm, $\ell_{2,1}$ norm, and Frobenius norm, it has the ability to capture the underlying noise distribution to a certain extent. Moreover, it incorporates learnable parameters that can adaptively adjust during optimization, enabling more effective modeling of complex noise patterns, especially in scenarios involving incomplete views. The DMR term is explicitly decomposed into two complementary components for better interpretability. Specifically, we define $\|\{\mathbf{Z}^v\}_{v=1}^m\|_{\text{DMR-1}}=\sum_{v=1}^m\sum_{v'=1,v'\neq v}^m\mathrm{Tr}\left(\mathbf{Z}^v\mathbf{L}^{v'}(\mathbf{Z}^v)^\top\right)$, and $\|\{\mathbf{Z}^v\}_{v=1}^m\|_{\text{DMR-2}}=\sum_{v=1}^m\mathrm{Tr}\left(\mathbf{Z}^v\mathbf{L}_\mathbf{s}(\mathbf{Z}^v)^\top\right)$. The combined effect of λ_2 and λ_3 can be regarded as equivalent to adjusting both the value of γ and the weight of the DMR term. $\|\{\mathbf{Z}^v\}_{v=1}^m\|_{\text{DMR-1}}$ encourages the manifolds of each view to mutually constrain each other, thus enhancing cross-view consistency. $\|\{\mathbf{Z}^v\}_{v=1}^m\|_{\text{DMR-2}}$ constructs a consensus Laplacian matrix that fuses the manifolds across all views, which helps capture a unified and globally consistent manifold structure. After optimization, we compute the left singular vectors of $\frac{1}{\sqrt{m}}[(\mathbf{Z}^1)^\top,\ldots,(\mathbf{Z}^m)^\top]$, and then apply spectral clustering on these vectors to obtain the final clustering result [38].

3.2 Optimazition

To solve the proposed optimization problem, we adopt the Alternating Direction Method of Multipliers (ADMM) [39]. The corresponding augmented Lagrangian function is formulated as follows:

$$\begin{aligned}&\mathcal{L}(\{\mathbf{A}^v\}_{v=1}^m,\{\mathbf{E}^v\}_{v=1}^m,\{\mathbf{Z}^v\}_{v=1}^m,\{\boldsymbol{\Sigma}^v\}_{v=1}^m,\{\mathbf{Y}^v\}_{v=1}^m,\boldsymbol{\mathcal{G}},\boldsymbol{\mathcal{Q}})\\ &=\|\boldsymbol{\mathcal{G}}\|_{\mathrm{HP}\ell_\delta}-\lambda_1\sum_{v=1}^m\left(\sum_{q=1}^n\ln(\mathcal{N}(\mathbf{e}_q^v\mid\mathbf{0},\boldsymbol{\Sigma}^v))\right)+\langle\boldsymbol{\mathcal{Q}},\boldsymbol{\mathcal{Z}}-\boldsymbol{\mathcal{G}}\rangle\\ &\quad+\sum_{v=1}^m\left(\langle\mathbf{Y}^v,\mathbf{X}^v-\mathbf{A}^v\mathbf{Z}^v-\mathbf{E}^v\rangle+\frac{\mu}{2}\|\mathbf{X}^v-\mathbf{A}^v\mathbf{Z}^v-\mathbf{E}^v\|_F^2\right)\\ &\quad+\frac{\rho}{2}\|\boldsymbol{\mathcal{Z}}-\boldsymbol{\mathcal{G}}\|_F^2+\lambda_2\sum_{v=1}^m\sum_{\substack{v'=1\\v'\neq v}}^m\mathrm{Tr}(\mathbf{Z}^v\mathbf{L}^{v'}(\mathbf{Z}^v)^\top)+\lambda_3\sum_{v=1}^m\mathrm{Tr}(\mathbf{Z}^v\mathbf{L}_\mathbf{s}(\mathbf{Z}^v)^\top)\end{aligned} \tag{7}$$

In the above formulation, $\{\mathbf{Y}^v\}_{v=1}^m$ and $\boldsymbol{\mathcal{Q}}$ are the Lagrange multipliers and $\mu>0$ and $\rho>0$ are the penalty parameters. The detailed optimization procedure is provided in Appendix A.4.

3.3 Convergence analysis

Theoretical guarantees for the convergence of the optimization algorithm are provided in Theorem 1, while Appendix A.5 offers a detailed exposition of the underlying principles and implementation details.

Theorem 1 *The sequence $\{\mathcal{J}_p=\mathbf{A}_p^v,\mathbf{E}_p^v,\mathbf{Z}_p^v,\boldsymbol{\Sigma}_p^v,\mathbf{Y}_p^v,\boldsymbol{\mathcal{G}}_p,\boldsymbol{\mathcal{Q}}_p\}_{p=1}^\infty$ generated by the proposed optimization algorithm satisfies the following properties:*

- *The sequence $\{\mathcal{J}_p\}_{p=1}^\infty$ is bounded;*
- *Any accumulation point of $\{\mathcal{J}_p\}_{p=1}^\infty$ is a stationary point that satisfies the KKT conditions.*

3.4 Complexity analysis

The computational complexity of the proposed GUITAR model mainly arises from variable optimization. Specifically, the optimization involves five groups of variables, namely $\mathbf{A}^v$, $\mathbf{E}^v$, $\mathbf{Z}^v$, $\mathbf{\Sigma}^v$, and $\boldsymbol{\mathcal{G}}$, whose respective computational complexities are denoted as $\mathcal{O}(nd_vt + d_vt)$, $\mathcal{O}(nd_v^3)$, $\mathcal{O}(ntd_v + n^3)$, $\mathcal{O}(nd_v^2)$, and $\mathcal{O}(mntlog(mn) + m^2nt)$. Consequently, the overall computational complexity of GUITAR scales cubically with the number of data samples.

4 Experiments

In this section, we evaluate the effectiveness and robustness of the proposed model through a series of experiments. All experiments are conducted in MATLAB R2023b on a machine equipped with a 2.30 GHz i7-12650H CPU and 16GB RAM. Due to space limitations, a subset of experimental results is presented in the main text; additional experiments can be found in Appendix A.6.

4.1 Experimental settings

Datasets: We conduct experiments on six datasets: Yale3 [40], MSRC_v1 [41], EYaleB10 [42], COIL20MV, Mfeat [43], and Scene [44]. These datasets differ in both sample size and the number of views. Specifically, Yale3 contains 165 samples with 3 views; MSRC_v1 has 210 samples and 5 views; EYaleB10 includes 640 samples with 3 views; COIL20MV provides 1440 samples across 4 views; Mfeat consists of 2000 samples with 6 views; and Scene comprises 2688 samples described by 4 views.

Incomplete multi-view data construction: Incompleteness is introduced to the originally complete multi-view datasets by randomly setting a fraction of samples to zero, where the missing rate r is chosen from $\{0.1, 0.3, 0.5\}$ in each view. To ensure that every sample remains present in at least one view, we restore the data in one randomly selected view for samples missing across all views. All experiments, except those in Section 4.2, are conducted with $r = 0.5$.

Baselines: We compare our method with six baseline approaches: BSV (2001) [45–47], Concat [46, 47], PVC (2014) [48], IMVC-CBG (2022) [49], PSIMVC-PG (2024) [50], and SCSL (2024) [30]. For each method requiring hyperparameter tuning, we adjust the parameters within the recommended ranges. For our method, we search for the optimal values of λ_1, λ_2, and λ_3 from the set $\{10^{-3}, 10^{-2}, 10^{-1}, 10^0, 10^1\}$, while δ is tuned over $\{10^{-3}, 10^{-2}, 10^{-1}, 10^0\}$.

Evaluation metrics: Three evaluation metrics, Accuracy (ACC), Normalized Mutual Information (NMI), and Purity (PUR), are used to assess clustering performance. To ensure the reliability of the results, each method is executed five times during the evaluation process.

4.2 Clustering results

The performance comparison of clustering results is shown in Table 1, with the top-performing method in each dataset highlighted in **bold** and the second-best method underlined. The analysis of the clustering results leads to the following three conclusions:

(1) The proposed GUITAR method consistently demonstrates strong performance across different missing rates, clearly outperforming the second-best method. For example, at a missing rate of 0.5, our method achieves higher ACC scores than the runner-up by 16.89%, 12.86%, 5.35%, 33.51%, 24.12%, and 15.98% on the Yale3, MSRC_v1, EYaleB10, COIL20MV, Mfeat, and Scene datasets, respectively. Furthermore, even at lower missing rates, our method achieves competitive results. These findings demonstrate the robustness of our approach in the presence of complex noise and validate the effectiveness of the GRN component.

(2) Compared with recent matrix-based methods such as IMVC-CBG (2022), PSIMVC-PG (2024), and SCSL (2024), our tensor-based approach consistently achieves superior performance. This highlights that the HPℓ_δ regularization enables the tensor low-rank constraint to effectively capture high-order correlations.

Table 1: Clustering performance comparison under different missing rates.

Data	Methods \ Missing rate	0.1			0.3			0.5		
		ACC	NMI	PUR	ACC	NMI	PUR	ACC	NMI	PUR
Yale3	BSV	35.64±6.99	41.06±6.93	36.73±6.74	33.82±6.17	35.53±6.85	35.76±5.88	26.06±2.94	25.59±3.36	28.48±2.74
	Concat	31.76±11.65	31.99±12.17	34.30±11.25	28.12±4.57	28.98±6.48	30.42±5.01	22.55±5.82	20.43±6.90	24.48±5.40
	PVC	50.30±2.54	53.58±2.06	51.27±1.80	39.74±2.22	43.10±1.43	40.90±2.19	40.44±1.86	42.82±1.55	42.22±2.16
	IMVC-CBG	44.48±0.33	45.75±0.00	45.09±0.33	37.58±0.00	38.55±0.00	38.79±0.00	22.91±0.27	19.42±0.29	23.52±0.27
	PSIMVC-PG	52.73±0.00	56.24±0.00	53.94±0.00	31.39±0.66	35.22±1.06	32.97±0.81	19.39±0.00	18.38±0.00	21.82±0.00
	SCSL	63.03±0.00	64.79±0.00	63.03±0.00	55.76±0.00	58.61±0.00	55.76±0.00	32.12±0.00	35.75±0.00	33.94±0.00
	GUITAR	**64.48±4.19**	**65.92±3.18**	**64.61±4.42**	**62.18±2.99**	**62.64±1.64**	**62.18±2.99**	**57.33±2.66**	**58.71±2.21**	**57.58±3.12**
MSRC_v1	BSV	60.00±9.61	51.44±5.29	62.86±6.01	40.10±4.71	28.93±3.48	41.81±3.99	31.43±3.10	18.12±2.97	32.19±3.06
	Concat	73.33±10.43	66.58±7.61	74.29±9.39	54.29±7.66	47.78±5.41	56.86±6.41	44.10±2.58	33.60±4.19	44.86±2.78
	PVC	62.78±5.77	49.46±3.47	64.98±3.36	71.24±5.34	59.36±3.80	71.96±4.53	52.25±9.29	46.75±8.86	56.75±8.47
	IMVC-CBG	50.19±0.43	41.06±0.75	52.10±0.64	36.67±0.00	24.83±0.00	37.62±0.00	19.05±0.00	4.80±0.00	19.05±0.00
	PSIMVC-PG	46.67±0.00	36.14±0.00	47.62±0.00	28.76±0.26	17.34±0.26	29.71±0.26	18.29±0.43	5.50±0.44	19.33±0.43
	SCSL	74.76±0.00	64.82±0.00	74.76±0.00	61.90±0.00	56.05±0.00	66.19±0.00	67.14±0.00	61.87±0.00	70.48±0.00
	GUITAR	**77.14±1.75**	**67.26±1.75**	**77.14±1.75**	**81.05±1.63**	**67.93±1.69**	**81.05±1.63**	**80.00±0.00**	**65.94±0.00**	**80.00±0.00**
EYaleB10	BSV	25.44±1.00	23.32±2.42	27.81±0.98	18.09±0.92	7.62±1.20	18.81±1.16	21.53±1.37	14.28±1.77	22.81±1.38
	Concat	17.53±2.24	6.83±3.47	19.03±2.92	18.59±1.57	8.13±2.56	19.47±1.94	16.94±2.05	5.40±1.98	17.75±1.73
	PVC	36.25±5.47	**35.07±7.80**	37.76±4.71	31.09±1.21	27.32±2.40	32.75±1.56	30.40±2.44	25.56±3.89	31.73±2.59
	IMVC-CBG	33.94±0.13	28.47±0.11	34.72±0.13	27.19±0.11	18.61±0.00	28.13±0.11	17.25±0.14	7.86±0.12	18.66±0.14
	PSIMVC-PG	30.09±0.00	23.88±0.12	31.34±0.00	24.06±0.00	15.20±0.00	24.69±0.00	17.03±0.00	8.78±0.00	19.53±0.00
	SCSL	12.81±0.00	3.31±0.00	13.13±0.00	12.19±0.00	2.72±0.00	12.50±0.00	20.00±0.00	8.42±0.00	20.78±0.00
	GUITAR	**37.03±0.96**	34.39±1.52	**37.97±0.95**	**37.97±0.63**	**34.68±0.68**	**38.91±0.46**	**35.75±1.37**	**30.30±2.01**	**36.41±1.48**
COIL20MV	BSV	52.81±4.93	65.04±2.26	56.89±4.05	42.06±3.63	49.45±1.51	44.82±2.85	31.74±1.95	37.18±1.58	33.93±1.86
	Concat	58.68±7.56	73.38±3.21	63.65±6.47	47.47±1.97	58.62±1.44	51.32±1.72	37.67±3.54	47.53±3.99	41.08±3.09
	PVC	5.05±0.00	0.00 ± 0.00	5.05 ± 0.00	5.29 ± 0.00	0.00 ± 0.00	5.29 ± 0.00	5.65 ± 0.00	0.00 ± 0.00	5.65 ± 0.00
	IMVC-CBG	56.51±1.30	67.58±0.59	59.63±0.85	50.90±0.47	58.12±0.28	54.61±0.26	41.00±1.40	50.45±1.00	44.18±1.29
	PSIMVC-PG	56.79±1.85	67.84±0.53	60.08±1.25	50.69±0.16	58.01±0.22	54.42±0.35	32.81±0.57	39.39±0.42	36.44±0.50
	SCSL	26.81±0.00	28.51±0.00	30.00±0.00	52.71±0.00	62.34±0.00	53.26±0.00	40.69±0.00	51.00±0.00	46.32±0.00
	GUITAR	**74.11±1.69**	**82.67±0.71**	**75.40±1.08**	**72.53±2.02**	**81.90±1.36**	**73.96±2.18**	**74.51±5.95**	**82.46±2.78**	**75.89±4.93**
Mfeat	BSV	63.22±6.56	60.32±4.60	67.42±6.05	52.70±4.46	48.51±2.18	54.19±3.60	39.21±4.00	33.07±2.87	41.68±3.13
	Concat	75.25±11.82	**73.15±6.24**	77.89±8.65	57.88±5.73	53.11±2.11	59.12±4.62	41.24±3.71	35.48±4.75	42.62±3.45
	PVC	66.80±2.83	59.58±1.07	68.08±1.89	64.26±3.36	53.93±2.00	65.21±2.21	58.19±4.47	49.29±3.89	59.20±4.21
	IMVC-CBG	53.50±0.00	48.31±0.00	53.90±0.00	35.20±0.00	26.49±0.00	35.50±0.00	20.95±0.00	11.54±0.00	21.40±0.00
	PSIMVC-PG	48.56±0.00	45.04±0.00	49.96±0.00	31.84±0.00	25.84±0.00	33.34±0.00	19.25±0.00	10.07±0.00	19.55±0.00
	SCSL	30.55±0.00	21.68±0.00	33.35±0.00	21.10±0.00	12.51±0.00	24.25±0.00	22.50±0.00	14.43±0.00	26.05±0.00
	GUITAR	**78.05±2.66**	71.53±1.10	**78.07±2.65**	**81.32±0.29**	**73.49±0.23**	**81.32±0.29**	**82.31±0.00**	**71.89±0.00**	**82.31±0.00**
Scene	BSV	51.18±1.22	37.62±0.82	54.47±0.98	43.09±2.88	29.30±1.99	45.20±2.63	32.65±2.75	19.58±1.80	34.54±2.32
	Concat	56.96±4.02	44.25±1.45	58.04±2.48	44.75±1.26	29.98±2.59	45.48±1.71	36.95±2.01	22.59±0.87	37.54±1.88
	PVC	55.00±2.40	42.46±2.58	56.18±2.13	46.78±3.36	38.14±2.73	50.57±3.61	42.02±1.06	31.75±1.82	43.75±0.87
	IMVC-CBG	42.37±0.00	29.10±0.00	44.90±0.00	27.49±0.00	14.77±0.00	29.24±0.00	20.50±0.00	6.19±0.00	21.24±0.00
	PSIMVC-PG	33.82±0.00	21.20±0.00	35.90±0.00	26.90±0.00	13.19±0.00	28.72±0.00	20.19±0.00	5.19±0.00	20.86±0.00
	SCSL	48.81±0.00	36.90±0.00	49.26±0.00	16.78±0.00	1.87±0.00	17.04±0.00	19.57±0.00	6.65±0.00	21.50±0.00
	GUITAR	**59.34±1.06**	**44.88±0.71**	**59.72±0.95**	**59.83±0.00**	**43.79±0.00**	**59.89±0.00**	**58.00±0.33**	**39.02±0.18**	**58.00±0.33**

(3) Whether compared with methods without manifold constraints (BSV, Concat, PVC, IMVC-CBG, PSIMVC-PG) or the manifold-constrained method SCSL, our approach maintains relatively stable performance across different datasets and missing rates. This can be attributed to the ability of DMR to accurately learn the underlying manifolds, even under high levels of missing data.

4.3 Parameters analysis

The GUITAR model involves three balancing parameters: λ_1, λ_2, and λ_3. To evaluate the sensitivity of the model to these parameters, we perform a grid search over two parameters while fixing the third, with search values drawn from $\{10^{-3}, 10^{-2}, 10^{-1}, 10^{0}, 10^{1}\}$. ACC is used as the evaluation criterion. As illustrated in Figure 2, the performance on the Mfeat dataset remains consistently stable when λ_1, λ_2, and λ_3 are chosen from $\{10^{-3}, 10^{-2}, 10^{-1}\}$.

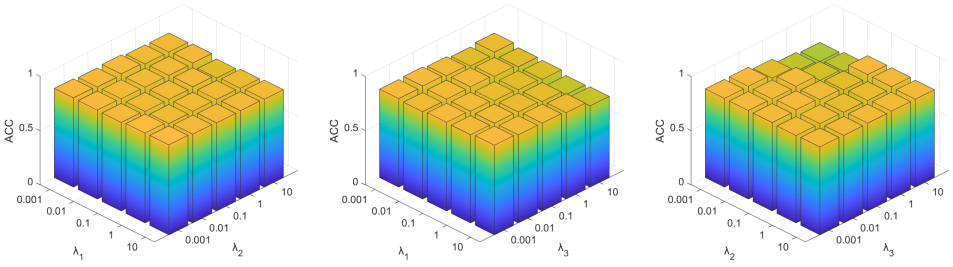

(a) λ_1 vs. λ_2 (b) λ_1 vs. λ_3 (c) λ_2 vs. λ_3

Figure 2: Sensitivity analysis of balancing parameters in the GUITAR model on the Mfeat dataset.

4.4 Anchor analysis

The proposed GUITAR model utilizes discriminative anchors from the original data as a dictionary to improve computational efficiency. The number of anchors t is varied within the range $[c, 7c]$, where c denotes the number of clusters. The detailed clustering results are presented in Figure 3. It can be observed that even with a number of anchors much smaller than the total number of samples, competitive and relatively stable clustering performance is consistently achieved across different datasets. However, results indicate that more anchors do not guarantee better performance. While insufficient anchors limit the dictionary's expressiveness, causing high reconstruction error, too many increase the risk of selecting low-quality anchors that introduce noise and degrade performance. The number of anchors should therefore be optimized empirically. In general, the GUITAR model yields the best performance when the number of anchors is $2c$ or $3c$.

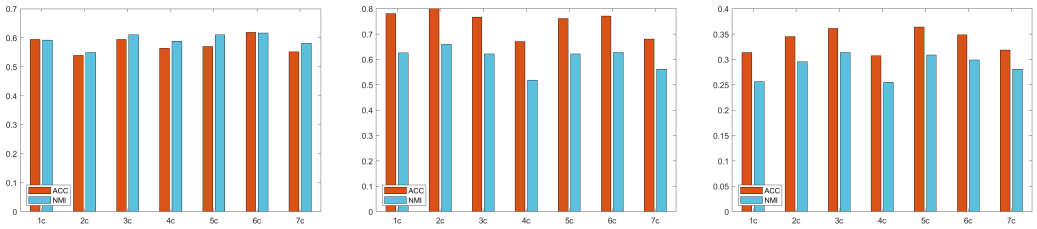

(a) Yale3 (b) MSRC_v1 (c) EYaleB10

Figure 3: The impact of anchor count on the GUITAR model.

4.5 Analysis of the HPℓ_δ parameter δ

In this section, we analyze the impact of the HPℓ_δ parameter on the performance of our model. We search for an optimal value of δ within the range $\{10^{-3}, 10^{-2}, 10^{-1}, 10^{0}\}$ to make HPℓ_δ more effective and compact. As shown in Figure 4, the performance metrics on the Yale3 dataset fluctuate as δ increases, while on the MSRC_v1 dataset they decrease, and on the EYaleB10 dataset they increase. For the other datasets, the performance remains relatively stable. Overall, the model achieves the best performance across all datasets when δ is set to 10^{-2}.

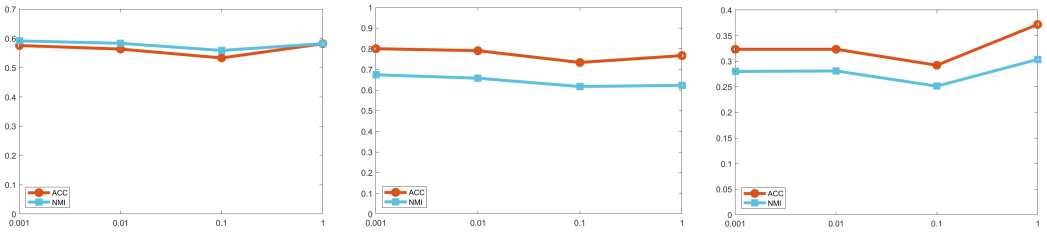

(a) Yale3 (b) MSRC_v1 (c) EYaleB10

Figure 4: The impact of δ on the GUITAR model.

4.6 Convergence behavior

We empirically validate the convergence of the GUITAR model using two metrics: the reconstruction error (RE), defined as $\min_v \|\mathbf{X}^v - \mathbf{A}^v\mathbf{Z}^v - \mathbf{E}^v\|_\infty$, and the match error (ME), given by $\|\boldsymbol{\mathcal{Z}} - \boldsymbol{\mathcal{G}}\|_\infty$. The convergence processes on the Yale3, EYaleB10, and COIL20MV datasets are illustrated in Figure 5. As shown, both RE and ME decrease rapidly and approach zero within 40 iterations, demonstrating the good convergence properties of the GUITAR model.

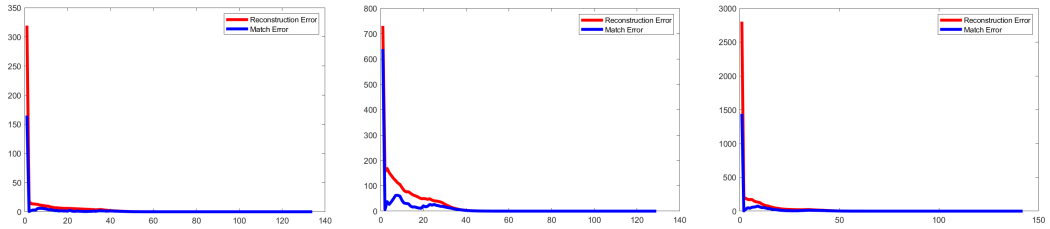

(a) Yale3 (b) EYaleB10 (c) COIL20MV

Figure 5: Convergence curves of the GUITAR model.

4.7 Ablation study

To study the effect of GRN and DMR on the model performance, we perform ablation by setting the balancing parameters λ_1, λ_2, and λ_3 to zero in different combinations. DMR can be decomposed into two smaller components: we define $\sum_{v=1}^{m} \sum_{v'=1, v' \neq v}^{m} \operatorname{Tr}\left(\mathbf{Z}^v \mathbf{L}^{v'} (\mathbf{Z}^v)^\top\right)$ as DMR-1, and $\sum_{v=1}^{m} \operatorname{Tr}\left(\mathbf{Z}^v \mathbf{L}_\mathbf{s} (\mathbf{Z}^v)^\top\right)$ as DMR-2. Table 2 reports the experimental results, where the best-performing entries are highlighted in **bold**. Removing GRN results in a substantial performance degradation, demonstrating its effectiveness in modeling complex noise. When GRN is present, incorporating either DMR-1 or DMR-2 leads to further improvements. The model achieves its optimal performance when GRN, DMR-1, and DMR-2 are all incorporated, indicating that the manifold learning capability of DMR also plays a crucial role in enhancing GUITAR.

Table 2: Ablation results of the GUITAR model.

Components / Datasets			Yale3			MSRC_v1			EYaleB10		
GRN	DMR-1	DMR-2	ACC	NMI	PUR	ACC	NMI	PUR	ACC	NMI	PUR
✓			43.03	48.84	44.24	26.67	13.91	28.57	16.88	5.73	17.81
	✓		7.88	10.91	15.15	14.76	2.99	17.14	10.16	1.45	11.41
		✓	7.88	10.91	15.15	24.29	5.13	24.76	10.16	1.45	11.41
✓	✓		52.12	56.70	52.73	72.86	56.72	72.86	36.72	29.89	38.28
✓		✓	50.30	52.74	50.30	75.71	59.12	75.71	27.66	20.56	29.84
	✓	✓	7.88	10.91	15.15	14.76	2.99	17.14	10.16	1.45	11.41
✓	✓	✓	**57.58**	**58.25**	**57.58**	**79.05**	**65.71**	**79.05**	**39.22**	**33.42**	**39.84**

5 Conclusion

This paper proposes a novel tensorized incomplete multi-view clustering framework that incorporates a Gaussian regression-based norm, along with two key enhancements: an improved, more compact and effective ℓ_δ norm, and a dual Laplacian manifold constraint designed to align and fuse view-specific manifolds. Our model introduces innovative formulations for noise modeling norms, rank functions for tensor low-rank regularization, and manifold constraints. Extensive experiments on six benchmark datasets demonstrate that our method consistently outperforms SOTA approaches, thereby validating the effectiveness and methodological novelty of GUITAR.

6 Limitations

The main limitation of the proposed model concerns its computational complexity. Specifically, the computational cost of GUITAR increases cubically with the number of data samples, primarily due to the matrix inversion required during the update of the coefficient matrices $\mathbf{Z}^v$. This complexity may limit the scalability of the model on large-scale datasets. Regarding hyperparameter sensitivity, our empirical analysis (see the corresponding chart) indicates that the model's performance exhibits moderate variation under different hyperparameter settings. This suggests that while the model is relatively robust, hyperparameter sensitivity still has a limited but non-negligible impact.

Acknowledgements

This work was supported by the Natural Science Foundation of Hebei Province (No. F2025205006), the Science Foundation of Hebei Normal University (No. L2025B38), and the Backbone Talent Program (Program for Returned Overseas Scholars) (No. A2025016).

References

[1] Jintian Ji and Songhe Feng. Anchors crash tensor: Efficient and scalable tensorial multi-view subspace clustering. *IEEE Transactions on Pattern Analysis and Machine Intelligence (TPAMI)*, 47(4):2660–2675, 2025.

[2] Wei Chang, Huimin Chen, Feiping Nie, Rong Wang, and Xuelong Li. Tensorized and compressed multi-view subspace clustering via structured constraint. *IEEE Transactions on Pattern Analysis and Machine Intelligence (TPAMI)*, 46(12):10434–10451, 2024.

[3] Hao Dai, Yang Liu, Peng Su, Hecheng Cai, Shudong Huang, and Jiancheng Lv. Multi-view clustering by inter-cluster connectivity guided reward. In *International Conference on Machine Learning (ICML)*, pages 9846–9855, 2024.

[4] Weixuan Liang, Chang Tang, Xinwang Liu, Yong Liu, Jiyuan Liu, En Zhu, and Kunlun He. On the consistency and large-scale extension of multiple kernel clustering. *IEEE Transactions on Pattern Analysis and Machine Intelligence(TPAMI)*, 46(10):6935–6947, 2024.

[5] Jiyuan Liu, Xinwang Liu, Chuankun Li, Xinhang Wan, Hao Tan, Yi Zhang, Weixuan Liang, Qian Qu, Yu Feng, Renxiang Guan, et al. Large-scale multi-view tensor clustering with implicit linear kernels. In *Proceedings of the IEEE/CVF Conference on Computer Vision and Pattern Recognition (CVPR)*, pages 20727–20736, 2025.

[6] Mouxing Yang, Yunfan Li, Peng Hu, Jinfeng Bai, Jiancheng Lv, and Xi Peng. Robust multi-view clustering with incomplete information. *IEEE Transactions on Pattern Analysis and Machine Intelligence (TPAMI)*, 45(1):1055–1069, 2023.

[7] Huayi Tang and Yong Liu. Deep safe incomplete multi-view clustering: Theorem and algorithm. In *International Conference on Machine Learning (ICML)*, pages 21090–21110, 2022.

[8] Jie Xu, Chao Li, Liang Peng, Yazhou Ren, Xiaoshuang Shi, Heng Tao Shen, and Xiaofeng Zhu. Adaptive feature projection with distribution alignment for deep incomplete multi-view clustering. *IEEE Transactions on Image Processing (TIP)*, 32:1354–1366, 2023.

[9] Jie Wen, Chengliang Liu, Gehui Xu, Zhihao Wu, Chao Huang, Lunke Fei, and Yong Xu. Highly confident local structure based consensus graph learning for incomplete multi-view clustering. In *Proceedings of the IEEE/CVF Conference on Computer Vision and Pattern Recognition (CVPR)*, pages 15712–15721, 2023.

[10] Siwei Wang, Xinwang Liu, Li Liu, Wenxuan Tu, Xinzhong Zhu, Jiyuan Liu, Sihang Zhou, and En Zhu. Highly-efficient incomplete largescale multiview clustering with consensus bipartite graph. In *Proceedings of the IEEE/CVF Conference on Computer Vision and Pattern Recognition (CVPR)*, pages 9766–9775, 2022.

[11] Xinwang Liu. Incomplete multiple kernel alignment maximization for clustering. *IEEE Transactions on Pattern Analysis and Machine Intelligence (TPAMI)*, 46(3):1412–1424, 2024.

[12] Jie Wen, Zheng Zhang, Zhao Zhang, Lei Zhu, Lunke Fei, Bob Zhang, and Yong Xu. Unified tensor framework for incomplete multi-view clustering and missing-view inferring. In *AAAI Conference on Artificial Intelligence (AAAI)*, pages 10273–10281, 2021.

[13] Tingting Wu, Songhe Feng, and Jiazheng Yuan. Low-rank kernel tensor learning for incomplete multi-view clustering. In *AAAI Conference on Artificial Intelligence (AAAI)*, pages 15952–15960, 2024.

[14] Zhibin Gu, Zhendong Li, and Songhe Feng. EDISON: Enhanced dictionary-induced tensorized incomplete multi-view clustering with gaussian error rank minimization. In *International Conference on Machine Learning (ICML)*, pages 16548–16567, 2024.

[15] Chao Zhang, Huaxiong Li, Wei Lv, Zizheng Huang, Yang Gao, and Chunlin Chen. Enhanced tensor low-rank and sparse representation recovery for incomplete multi-view clustering. In *AAAI Conference on Artificial Intelligence (AAAI)*, pages 11174–11182, 2023.

[16] Menglei Hu and Songcan Chen. Doubly aligned incomplete multi-view clustering. In *International Joint Conference on Artificial Intelligence (IJCAI)*, pages 2262–2268, 2018.

[17] Shengju Yu, Zhibin Dong, Siwei Wang, Xinhang Wan, Yue Liu, Weixuan Liang, Pei Zhang, Wenxuan Tu, and Xinwang Liu. Towards resource-friendly, extensible and stable incomplete multi-view clustering. In *International Conference on Machine Learning (ICML)*, pages 1–11, 2024.

[18] Yijie Lin, Yuanbiao Gou, Xiaotian Liu, Jinfeng Bai, Jiancheng Lv, and Xi Peng. Dual contrastive prediction for incomplete multi-view representation learning. *IEEE Transactions on Pattern Analysis and Machine Intelligence (TPAMI)*, 45(4):4447–4461, 2023.

[19] Zhenglai Li, Chang Tang, Xiao Zheng, Xinwang Liu, Wei Zhang, and En Zhu. High-order correlation preserved incomplete multi-view subspace clustering. *IEEE Transactions on Image Processing (TIP)*, 31:2067–2080, 2022.

[20] Yanyong Huang, Minghui Lu, Wei Huang, Xiuwen Yi, and Tianrui Li. TIME-FS: Joint learning of tensorial incomplete multi-view unsupervised feature selection and missing-view imputation. In *AAAI Conference on Artificial Intelligence (AAAI)*, pages 17503–17510, 2025.

[21] Xiaochun Cao, Changqing Zhang, Huazhu Fu, Si Liu, and Hua Zhang. Diversity-induced multi-view subspace clustering. In *Proceedings of the IEEE/CVF Conference on Computer Vision and Pattern Recognition (CVPR)*, pages 586–594, 2015.

[22] Wei Chang, Huimin Chen, Feiping Nie, Rong Wang, and Xuelong Li. Tensorized and compressed multi-view subspace clustering via structured constraint. *IEEE Transactions on Pattern Analysis and Machine Intelligence (TPAMI)*, 46(12):10434–10451, 2024.

[23] Suyuan Liu, Xinwang Liu, Siwei Wang, Xin Niu, and En Zhu. Fast incomplete multi-view clustering with view-independent anchors. *IEEE Transactions on Neural Networks and Learning Systems (TNNLS)*, 35(6):7740–7751, 2024.

[24] Pei Zhang, Siwei Wang, Liang Li, Changwang Zhang, Xinwang Liu, En Zhu, Zhe Liu, Lu Zhou, and Lei Luo. Let the data choose: Flexible and diverse anchor graph fusion for scalable multi-view clustering. In *Proceedings of the AAAI Conference on Artificial Intelligence (AAAI)*, pages 11262–11269, 2023.

[25] Jun Wang, Chang Tang, Zhiguo Wan, Wei Zhang, Kun Sun, and Albert Y. Zomaya. Efficient and effective one-step multiview clustering. *IEEE Transactions on Neural Networks and Learning Systems (TNNLS)*, 35(9):12224–12235, 2024.

[26] Junmin Liu, Yijun Chen, Jiangshe Zhang, and Zongben Xu. Enhancing low-rank subspace clustering by manifold regularization. *IEEE Transactions on Image Processing (TIP)*, 23(9):4022–4030, 2014.

[27] Baohua Li, Ying Zhang, Zhouchen Lin, and Huchuan Lu. Subspace clustering by mixture of gaussian regression. In *Proceedings of the IEEE/CVF Conference on Computer Vision and Pattern Recognition (CVPR)*, pages 2094–2102, 2015.

[28] Guang-Yu Zhang, Dong Huang, and Chang-Dong Wang. Unified and tensorized incomplete multi-view kernel subspace clustering. *IEEE Transactions on Emerging Topics in Computational Intelligence (TETCI)*, 8(2):1550–1566, 2024.

[29] Jintian Ji and Songhe Feng. Anchor structure regularization induced multi-view subspace clustering via enhanced tensor rank minimization. In *Proceedings of the IEEE/CVF International Conference on Computer Vision (ICCV)*, pages 19343–19352, 2023.

[30] Suyuan Liu, Junpu Zhang, Yi Wen, Xihong Yang, Siwei Wang, Yi Zhang, En Zhu, Chang Tang, Long Zhao, and Xinwang Liu. Sample-level cross-view similarity learning for incomplete multi-view clustering. In *Proceedings of the AAAI Conference on Artificial Intelligence (AAAI)*, pages 14017–14025, 2024.

[31] Yuan Xie, Dacheng Tao, Wensheng Zhang, Yan Liu, Lei Zhang, and Yanyun Qu. On unifying multi-view self-representations for clustering by tensor multi-rank minimization. *International Journal of Computer Vision (IJCV)*, 126:1157–1179, 2018.

[32] Chong Peng, Zhao Kang, Ming Yang, and Qiang Cheng. Feature selection embedded subspace clustering. *IEEE Signal Processing Letters (SPL)*, 23(7):1018–1022, 2016.

[33] Maryam Fazel, Haitham Hindi, and Stephen P Boyd. Log-det heuristic for matrix rank minimization with applications to hankel and euclidean distance matrices. In *Proceedings of the 2003 American Control Conference (ACC)*, volume 3, pages 2156–2162. IEEE, 2003.

[34] Joshua Trzasko and Armando Manduca. Highly undersampled magnetic resonance image reconstruction via homotopic ℓ_0-minimization. *IEEE Transactions on Medical Imaging (TMI)*, 28(1):106–121, 2008.

[35] Yongyong Chen, Shuqin Wang, Xiaolin Xiao, Youfa Liu, Zhongyun Hua, and Yicong Zhou. Self-paced enhanced low-rank tensor kernelized multi-view subspace clustering. *IEEE Transactions on Multimedia (TMM)*, 24:4054–4066, 2021.

[36] Zhao Kang, Chong Peng, and Qiang Cheng. Robust pca via nonconvex rank approximation. In *2015 IEEE International Conference on Data Mining (ICDM)*, pages 211–220, 2015.

[37] Misha E Kilmer, Karen Braman, Ning Hao, and Randy C Hoover. Third-order tensors as operators on matrices: A theoretical and computational framework with applications in imaging. *SIAM Journal on Matrix Analysis and Applications (SIMAX)*, 34(1):148–172, 2013.

[38] Zhao Kang, Wangtao Zhou, Zhitong Zhao, Junming Shao, Meng Han, and Zenglin Xu. Large-scale multi-view subspace clustering in linear time. In *Proceedings of the AAAI Conference on Artificial Intelligence (AAAI)*, pages 4412–4419, 2020.

[39] Zhouchen Lin, Risheng Liu, and Zhixun Su. Linearized alternating direction method with adaptive penalty for low-rank representation. *Advances in Neural Information Processing Systems (NIPS)*, pages 1–9, 2011.

[40] Peter N. Belhumeur, Joao P Hespanha, and David J. Kriegman. Eigenfaces vs. fisherfaces: Recognition using class specific linear projection. *IEEE Transactions on pattern analysis and machine intelligence (TPAMI)*, 19(7):711–720, 1997.

[41] Wei Xia, Quanxue Gao, Qianqian Wang, Xinbo Gao, Chris Ding, and Dacheng Tao. Tensorized bipartite graph learning for multi-view clustering. *IEEE Transactions on Pattern Analysis and Machine Intelligence (TPAMI)*, 45(4):5187–5202, 2022.

[42] Guangcan Liu, Zhouchen Lin, and Yong Yu. Robust subspace segmentation by low-rank representation. In *Proceedings of the 27th International Conference on Machine Learning (ICML)*, pages 663–670, 2010.

[43] Feiping Nie, Lai Tian, and Xuelong Li. Multiview clustering via adaptively weighted procrustes. In *Proceedings of the 24th ACM SIGKDD International Conference on Knowledge Discovery & Data Mining (KDD)*, pages 2022–2030, 2018.

[44] Si-Guo Fang, Dong Huang, Xiao-Sha Cai, Chang-Dong Wang, Chaobo He, and Yong Tang. Efficient multi-view clustering via unified and discrete bipartite graph learning. *IEEE Transactions on Neural Networks and Learning Systems (TNNLS)*, 35(8):11436–11447, 2024.

[45] Andrew Ng, Michael Jordan, and Yair Weiss. On spectral clustering: Analysis and an algorithm. *Advances in Neural Information Processing Systems (NIPS)*, pages 1–8, 2001.

[46] Jie Wen, Zheng Zhang, Lunke Fei, Bob Zhang, Yong Xu, Zhao Zhang, and Jinxing Li. A survey on incomplete multiview clustering. *IEEE Transactions on Systems, Man, and Cybernetics: Systems (TSMC)*, 53(2):1136–1149, 2022.

[47] Jie Wen, Yong Xu, and Hong Liu. Incomplete multiview spectral clustering with adaptive graph learning. *IEEE Transactions on Cybernetics (TCYB)*, 50(4):1418–1429, 2018.

[48] Shao-Yuan Li, Yuan Jiang, and Zhi-Hua Zhou. Partial multi-view clustering. In *Proceedings of the AAAI Conference on Artificial Intelligence (AAAI)*, pages 1–7, 2014.

[49] Siwei Wang, Xinwang Liu, Li Liu, Wenxuan Tu, Xinzhong Zhu, Jiyuan Liu, Sihang Zhou, and En Zhu. Highly-efficient incomplete large-scale multi-view clustering with consensus bipartite graph. In *Proceedings of the IEEE/CVF Conference on Computer Vision and Pattern Recognition (CVPR)*, pages 9776–9785, 2022.

[50] Miaomiao Li, Siwei Wang, Xinwang Liu, and Suyuan Liu. Parameter-free and scalable incomplete multiview clustering with prototype graph. *IEEE Transactions on Neural Networks and Learning Systems (TNNLS)*, 35(1):300–310, 2022.

[51] Pham Dinh Tao and LT Hoai An. Convex analysis approach to dc programming: theory, algorithms and applications. *Acta mathematica vietnamica*, 22(1):289–355, 1997.

[52] Adrian S Lewis and Hristo S Sendov. Nonsmooth analysis of singular values. part i: Theory. *Set-Valued Analysis*, 13:213–241, 2005.

[53] Robert G Bartle and Donald R Sherbert. *Introduction to real analysis*. John Wiley & Sons, Inc., 2000.

A Technical Appendices and Supplementary Material

The supplementary material provides deeper insights into the GUITAR model through detailed optimization procedures, a convergence proof, additional experimental results, and further analyses.

A.1 Construction of the Gaussian Regression Norm

$\mathcal{N}(\mathbf{e}_q^v \mid \boldsymbol{\mu}^v, \boldsymbol{\Sigma}^v)$ can be characterized by its probability density function, namely, $\mathcal{N}(\mathbf{e}_q^v \mid \boldsymbol{\mu}^v, \boldsymbol{\Sigma}^v) = \frac{1}{(2\pi)^{d_v/2}|\boldsymbol{\Sigma}^v|^{1/2}} \exp\left(-\frac{1}{2}(\mathbf{e}_q^v - \boldsymbol{\mu}^v)^\top (\boldsymbol{\Sigma}^v)^{-1}(\mathbf{e}_q^v - \boldsymbol{\mu}^v)\right)$. The Gaussian Regression Norm is derived by the negative log-likelihood of the noise under a multivariate Gaussian model. Specifically, let $\mathbf{e}_q^v$ denote the noise vector of the q-th sample in the v-th view, which is assumed to follow a multivariate Gaussian distribution:

$$p(\mathbf{e}_q^v) = \mathcal{N}(\mathbf{e}_q^v \mid \boldsymbol{\mu}^v, \boldsymbol{\Sigma}^v) \tag{8}$$

where $\boldsymbol{\mu}^v$ and $\boldsymbol{\Sigma}^v$ represent the mean vector and covariance matrix for the v-th view, respectively. Assuming that the noise vectors within each view are independent, the likelihood of the entire noise matrix $\mathbf{E}^v = [\mathbf{e}_1^v, \cdots, \mathbf{e}_n^v]$ can be expressed as:

$$p(\mathbf{E}^v) = \prod_{q=1}^{n} \mathcal{N}(\mathbf{e}_q^v \mid \boldsymbol{\mu}^v, \boldsymbol{\Sigma}^v) \tag{9}$$

Taking the negative logarithm yields the negative log-likelihood for the v-th view:

$$-\ln p(\mathbf{E}^v) = -\sum_{q=1}^{n} \ln\left(\mathcal{N}(\mathbf{e}_q^v \mid \boldsymbol{\mu}^v, \boldsymbol{\Sigma}^v)\right) \tag{10}$$

To regularize the noise across all views, we minimize the sum of negative log-likelihoods over all m views, which leads to the definition of the Gaussian Regression Norm:

$$\|\{\mathbf{E}^v\}_{v=1}^m\|_{\mathrm{GRN}} = \sum_{v=1}^{m}(-\ln p(\mathbf{E}^v)) = -\sum_{v=1}^{m}\left(\sum_{q=1}^{n} \ln\left(\mathcal{N}(\mathbf{e}_q^v \mid \boldsymbol{\mu}^v, \boldsymbol{\Sigma}^v)\right)\right) \tag{11}$$

A.2 Detailed analysis of the Dual Manifold Regularization

The Dual Manifold Regularization has been introduced in the main text; however, certain details were not fully elaborated due to space limitations. This subsection will provide a further analysis.

Detailed explanation of Dual Manifold Regularization: The first term in the DMR, $\sum_{v=1}^{m}\sum_{v'=1,v'\neq v}^{m}\mathrm{Tr}\left(\mathbf{Z}^{v}\mathbf{L}^{v'}(\mathbf{Z}^{v})^{\top}\right)$, is designed to enforce cross-view manifold alignment. Specifically, it encourages the representation $\mathbf{Z}^{v}$ of each view to conform to the manifold structure captured by the Laplacian matrix $\mathbf{L}^{v'}$ of other views. This mutual regularization narrows the discrepancy between views and enhances the overall consistency among them. The second term, $\sum_{v=1}^{m}\mathrm{Tr}\left(\mathbf{Z}^{v}\mathbf{L}_{\mathbf{s}}(\mathbf{Z}^{v})^{\top}\right)$, incorporates a consensus Laplacian matrix $\mathbf{L}_{\mathbf{s}}$ that fuses the manifold structures from all views. It plays a complementary role by guiding each view's representation toward a globally consistent manifold, which reflects the intrinsic geometry shared across views.

Distinctions between the two terms in DMR: The two terms in the DMR serve complementary but distinct roles in promoting consistent manifold learning across views. When the manifold structures across different views differ significantly, enforcing a unified manifold directly may introduce bias. This issue is addressed by the first term, $\sum_{v=1}^{m}\sum_{v'=1,v'\neq v}^{m}\mathrm{Tr}\left(\mathbf{Z}^{v}\mathbf{L}^{v'}(\mathbf{Z}^{v})^{\top}\right)$, which imposes cross-view constraints, encouraging the manifold of each view to align with those of the others. This mutual regularization helps to reduce discrepancies among view-specific manifolds and improves inter-view consistency. In contrast, the second term, $\sum_{v=1}^{m}\mathrm{Tr}\left(\mathbf{Z}^{v}\mathbf{L}_{\mathbf{s}}(\mathbf{Z}^{v})^{\top}\right)$, constructs a consensus Laplacian matrix by integrating the manifold structures of all views. Its goal is to capture a globally consistent and representative manifold structure shared across views. The effectiveness of this consensus term is enhanced when the individual view manifolds are already well-aligned, a condition facilitated by the first term. Together, these two terms enable the model to first harmonize local structures and then learn a unified global manifold.

A.3 Analysis of the High-Preservation ℓ_δ-norm mechanism

Theoretical analysis: Let the function $f_{HP\ell_\delta}(x)=\frac{(1+\delta)\tanh x}{\delta+\tanh x}$. As $x\to 0$, we have $f_{HP\ell_\delta}(x)\to 0$. When $x\to+\infty$, since $\tanh(x)\to\frac{\pi}{2}$, the function converges to $f_{HP\ell_\delta}(x)\to\frac{\pi}{2\delta+\pi}<1$.For comparison, consider $f_{\ell_\delta}(x)=\frac{(1+\delta)x}{\delta+x}$. When $x\to 0$, $\tanh(x)\approx x$, so $f_{HP\ell_\delta}(x)\approx f_{\ell_\delta}(x)$, indicating that the penalization on small singular values remains almost unchanged. However, as $x\to+\infty$, $f_{\ell_\delta}(x)\to 1$, while $f_{HP\ell_\delta}(x)$ converges to a fixed value $\frac{\pi}{2\delta+\pi}$ strictly less than 1. This upper saturation effect effectively suppresses the penalization on large singular values, thus preserving more dominant components. As a result, the HPℓ_δ-norm penalizes small singular values effectively while reducing shrinkage on large ones, achieving a desirable balance between low-rankness and the preservation of critical information.

Empirical analysis: To empirically validate the effectiveness of the proposed HPℓ_δ norm, we conduct comparative experiments by replacing it with the LogDet function, the Laplace function, and the standard ℓ_δ norm. All evaluations are carried out on the benchmark datasets with a missing rate of 0.5, and each experiment is executed five times during the evaluation process. As shown in Table 3, the proposed HP-ℓ_δ norm achieves superior or competitive performance across most datasets, demonstrating its effectiveness.

Table 3: Comparative experimental results of different methods.

Datasets	Yale3	MSRC_v1	EYaleB10	COIL20MV	Mfeat	Scene
LogDet	56.97 ± 2.94	76.19 ± 0.00	35.78 ± 1.10	71.65 ± 2.67	81.83 ± 0.00	54.47 ± 0.46
Laplace	55.88 ± 1.45	76.76 ± 1.03	37.16 ± 2.05	72.75 ± 3.89	82.11 ± 0.00	**58.35 ± 0.17**
ℓ_δ	54.91 ± 2.29	79.52 ± 0.58	35.84 ± 2.09	74.50 ± 3.44	81.47 ± 0.11	57.66 ± 0.00
HP-ℓ_δ	**57.33 ± 2.66**	**80.00 ± 0.00**	**38.16 ± 2.05**	**74.51 ± 5.95**	**82.31 ± 0.00**	58.09 ± 0.00

A.4 Optimization procedures

The augmented Lagrangian function to be optimized is formulated as follows:

$$\begin{aligned}
&\mathcal{L}(\{\mathbf{A}^v\}_{v=1}^m, \{\mathbf{E}^v\}_{v=1}^m, \{\mathbf{Z}^v\}_{v=1}^m, \{\mathbf{\Sigma}^v\}_{v=1}^m, \{\mathbf{Y}^v\}_{v=1}^m, \boldsymbol{\mathcal{G}}, \boldsymbol{\mathcal{Q}}) \\
&= \|\boldsymbol{\mathcal{G}}\|_{\mathrm{HP}\ell_\delta} - \lambda_1 \sum_{v=1}^{m} \left(\sum_{q=1}^{n} \ln(\mathcal{N}(\mathbf{e}_q^v \mid \mathbf{0}, \mathbf{\Sigma}^v)) \right) + \langle \boldsymbol{\mathcal{Q}}, \boldsymbol{\mathcal{Z}} - \boldsymbol{\mathcal{G}} \rangle \\
&\quad + \sum_{v=1}^{m} \left(\langle \mathbf{Y}^v, \mathbf{X}^v - \mathbf{A}^v \mathbf{Z}^v - \mathbf{E}^v \rangle + \frac{\mu}{2} \|\mathbf{X}^v - \mathbf{A}^v \mathbf{Z}^v - \mathbf{E}^v\|_F^2 \right) \\
&\quad + \frac{\rho}{2} \|\boldsymbol{\mathcal{Z}} - \boldsymbol{\mathcal{G}}\|_F^2 + \lambda_2 \sum_{v=1}^{m} \sum_{\substack{v'=1 \\ v' \neq v}}^{m} \mathrm{Tr}(\mathbf{Z}^v \mathbf{L}^{v'} (\mathbf{Z}^v)^\top) + \lambda_3 \sum_{v=1}^{m} \mathrm{Tr}(\mathbf{Z}^v \mathbf{L}_\mathbf{s} (\mathbf{Z}^v)^\top)
\end{aligned} \tag{12}$$

Eq. (12) can be reformulated as a set of the following subproblems.

$\mathbf{A}^v$-Subproblem With other variables held constant, $\mathbf{A}^v$ can be obtained by solving

$$\mathbf{A}^v = \underset{(\mathbf{A}^v)^\top \mathbf{A}^v = \mathbf{I}}{arg\,max} \ \mathrm{Tr}((\mathbf{A}^v)^\top \mathbf{M}^v) \tag{13}$$

where $\mathbf{M}^v = (\mathbf{Y}^v + \mu \mathbf{X}^v - \mu \mathbf{E}^v)(\mathbf{Z}^v)^\top$. To obtain the optimal $\mathbf{A}^v$, singular value decomposition (SVD) is performed on $\mathbf{M}^v$, yielding $\mathbf{U}_{\mathbf{A}^v}$ and $\mathbf{V}_{\mathbf{A}^v}^\top$, which are the left and right singular matrices of $\mathbf{M}^v$, respectively. The product $\mathbf{U}_{\mathbf{A}^v} \mathbf{V}_{\mathbf{A}^v}^\top$ then gives the optimal solution for $\mathbf{A}^v$.

$\mathbf{E}^v$-Subproblem With other variables fixed, $\mathbf{E}^v \in \mathbb{R}^{d_v \times n}$ is updated column-wise, where the q-th column $\mathbf{e}_q^v$ represents the noise corresponding to the q-th sample of the v-th view, and can be obtained by solving the following optimization problem:

$$\begin{aligned}
&\underset{\mathbf{e}_q^v}{min} \ -\lambda_1 \ln \left(\mathcal{N}(\mathbf{e}_q^v | \mathbf{0}, \mathbf{\Sigma}^v) \right) + \left\langle \mathbf{y}_q^v, \mathbf{x}_q^v - \mathbf{A}^v \mathbf{z}_q^v - \mathbf{e}_q^v \right\rangle \\
&+ \frac{\mu}{2} \|\mathbf{x}_q^v - \mathbf{A}^v \mathbf{z}_q^v - \mathbf{e}_q^v\|_2^2
\end{aligned} \tag{14}$$

The optimal solution is given by

$$\mathbf{e}_q^v = \left(\lambda_1 (\mathbf{\Sigma}^v)^{-1} + \mu \mathbf{I} \right)^{-1} \left[\mathbf{y}_q^v - \mu (\mathbf{A}^v \mathbf{z}_q^v - \mathbf{x}_q^v) \right] \tag{15}$$

In this context, $\mathbf{y}_q^v$, $\mathbf{z}_q^v$, and $\mathbf{x}_q^v$ correspond to the q-th column vectors of the matrices $\mathbf{Y}^v \in \mathbb{R}^{d_v \times n}$, $\mathbf{Z}^v \in \mathbb{R}^{t \times n}$, and $\mathbf{X}^v \in \mathbb{R}^{d_v \times n}$, respectively.

$\mathbf{\Sigma}^v$-Subproblem With other variables fixed, the update of $\mathbf{\Sigma}^v$ can be formulated as

$$\min_{\mathbf{\Sigma}^v} \ -\lambda_1 \sum_{q=1}^{n} \ln \left(\mathcal{N}\left(\mathbf{e}_q^v \mid \mathbf{0}, \mathbf{\Sigma}^v\right) \right). \tag{16}$$

This optimization problem admits a closed-form solution, resulting in the following update for the covariance matrix $\mathbf{\Sigma}^v$:

$$\mathbf{\Sigma}^v = \frac{1}{n} \left(\sum_{q=1}^{n} \mathbf{e}_q^v (\mathbf{e}_q^v)^\top + \epsilon \mathbf{I} \right) \tag{17}$$

where $\epsilon \mathbf{I}$ is a small regularization term added to ensure numerical stability.

$\mathbf{Z}^v$-Subproblem With other variables fixed, the update of $\mathbf{Z}^v$ is formulated as the following optimization problem:

$$\begin{aligned}\mathbf{Z}^v = \underset{\mathbf{Z}^v}{arg\,min}\ & \operatorname{Tr}(\mathbf{Q}^{v\top}(\mathbf{Z}^v - \mathbf{G}^v)) + \frac{\rho}{2}\|\mathbf{Z}^v - \mathbf{G}^v\|_F^2 \\ & + \langle \mathbf{Y}^v, \mathbf{X}^v - \mathbf{A}^v\mathbf{Z}^v - \mathbf{E}^v\rangle + \frac{\mu}{2}\|\mathbf{X}^v - \mathbf{A}^v\mathbf{Z}^v - \mathbf{E}^v\|_F^2 \\ & + \lambda_2 \sum_{\substack{v'=1 \\ v'\neq v}}^{m} \operatorname{Tr}(\mathbf{Z}^v\mathbf{L}^{v'}(\mathbf{Z}^v)^\top) + \lambda_3 \operatorname{Tr}(\mathbf{Z}^v\mathbf{L}_{\mathbf{s}}(\mathbf{Z}^v)^\top)\end{aligned} \tag{18}$$

By setting the derivative of the objective with respect to $\mathbf{Z}^v$ to zero, the following linear equation is obtained:

$$\mathbf{Z}^v\Big(\rho\mathbf{I} + \mu\mathbf{I} + 2\lambda_2 \sum_{\substack{v'=1 \\ v'\neq v}}^{m} \mathbf{L}^{v'} + 2\lambda_3\mathbf{L}_{\mathbf{s}}\Big) = \big(\rho\mathbf{G}^v - \mathbf{Q}^v + (\mathbf{A}^v)^\top\mathbf{Y}^v + \mu(\mathbf{A}^v)^\top(\mathbf{X}^v - \mathbf{E}^v)\big) \tag{19}$$

Therefore, the closed-form solution for $\mathbf{Z}^v$ is

$$\mathbf{Z}^v = \big(\rho\mathbf{G}^v - \mathbf{Q}^v + (\mathbf{A}^v)^\top\mathbf{Y}^v + \mu(\mathbf{A}^v)^\top(\mathbf{X}^v - \mathbf{E}^v)\big)\Big(\rho\mathbf{I} + \mu\mathbf{I} + 2\lambda_2 \sum_{\substack{v'=1 \\ v'\neq v}}^{m} \mathbf{L}^{v'} + 2\lambda_3\mathbf{L}_{\mathbf{s}}\Big)^{-1} \tag{20}$$

$\boldsymbol{\mathcal{G}}$-Subproblem With other variables fixed, $\boldsymbol{\mathcal{G}}$ can be obtained by solving

$$\boldsymbol{\mathcal{G}} = \underset{\boldsymbol{\mathcal{G}}}{arg\,min}\ \frac{1}{\rho}\|\boldsymbol{\mathcal{G}}\|_{\mathrm{HP}\ell_\delta} + \frac{1}{2}\|\boldsymbol{\mathcal{G}} - (\boldsymbol{\mathcal{Z}} + \frac{\boldsymbol{\mathcal{Q}}}{\rho})\|_F^2 \tag{21}$$

The optimal solution of $\boldsymbol{\mathcal{G}}$ can be obtained according to the following theorem:

Theorem 2 *Given a tensor $\boldsymbol{\mathcal{D}} \in \mathbb{R}^{n_1\times n_2\times n_3}$, whose tensor singular value decomposition (t-SVD) is denoted as $\boldsymbol{\mathcal{D}} = \boldsymbol{\mathcal{U}} * \boldsymbol{\mathcal{S}} * \boldsymbol{\mathcal{V}}^\top$, our objective is to address the following minimization problem involving the High-Preservation ℓ_δ-norm:*

$$\min_{\boldsymbol{\mathcal{G}}}\ \xi\|\boldsymbol{\mathcal{G}}\|_{HP\ell_\delta} + \frac{1}{2}\|\boldsymbol{\mathcal{G}} - \boldsymbol{\mathcal{D}}\|_F^2 \tag{22}$$

The optimal solution to Eq. (22) can be computed in closed-form as:

$$\boldsymbol{\mathcal{G}}^* = \boldsymbol{\mathcal{U}} * \mathit{ifft}\big(\Omega_{f,\xi}(\boldsymbol{\mathcal{S}}_f), [], 3\big) * \boldsymbol{\mathcal{V}}^\top \tag{23}$$

In this formulation, $\mathit{ifft}\big(\Omega_{f,\xi}(\boldsymbol{\mathcal{S}}_f), [], 3\big)$ denotes a tensor whose frontal slices are diagonal matrices. Each diagonal element $\Omega_{f,\xi}(\boldsymbol{\mathcal{S}}_f^k(i,i))$ is obtained by solving the following optimization problem:

$$\Omega_{f,\xi}(\boldsymbol{\mathcal{S}}_f^k(i,i)) = \underset{x\geq 0}{\arg\min}\ \frac{1}{2}\Big(x - \boldsymbol{\mathcal{S}}_f^k(i,i)\Big)^2 + \xi f(x) \tag{24}$$

where $\xi > 0$ and the function $f(x)$ is defined as $\frac{(1+\delta)\tanh x}{\delta+\tanh x}$.

Eq. (24) comprises both convex and concave components, and can be addressed using Difference of Convex (DC) programming [51], leading to the following closed-form solution:

$$\zeta^{iter+1} = \left(\boldsymbol{\mathcal{S}}_f^k(i,i) - \frac{\partial f(\zeta^{iter})}{\rho}\right)_+ \tag{25}$$

where $f(x) = \frac{(1+\delta)\tanh x}{\delta+\tanh x}$, $\zeta = \Omega_{f,\xi}(\boldsymbol{\mathcal{S}}_f^k(i,i))$, and $iter$ denotes the iteration index.

Lagrange multipliers and penalty parameters The Lagrange multipliers $\mathbf{Y}^v$, $\boldsymbol{\mathcal{Q}}$, and the penalty parameters μ, ρ are updated according to the following rules:

$$\begin{cases} \mathbf{Y}^v = \mathbf{Y}^v + \mu(\mathbf{X}^v - \mathbf{A}^v\mathbf{Z}^v - \mathbf{E}^v) \\ \boldsymbol{\mathcal{Q}} = \boldsymbol{\mathcal{Q}} + \rho(\boldsymbol{\mathcal{Z}} - \boldsymbol{\mathcal{G}}) \\ \mu = \eta_\mu \mu, \mu = min(\mu, \mu_{max}) \\ \rho = \eta_\rho \rho, \rho = min(\rho, \rho_{max}) \end{cases} \tag{26}$$

With the ADMM-based optimization procedure concluded, the subsequent updates are carried out independently of the ADMM scheme.

Update $\mathbf{L}^v$

$$\mathbf{L}^v = \mathbf{I} - (\mathbf{D}^v)^{-1/2}\mathbf{S}^v(\mathbf{D}^v)^{-1/2} \tag{27}$$

The Laplacian matrix $\mathbf{L}^v$ is constructed from the similarity matrix $\mathbf{S}^v \in \mathbb{R}^{n\times n}$ for view v. Specifically, $\mathbf{S}^v_{ij} = \frac{(\mathbf{z}^v_i)^\top \mathbf{z}^v_j}{\|\mathbf{z}^v_i\|_2 \cdot \|\mathbf{z}^v_j\|_2}$, where $\mathbf{z}^v_i \in \mathbb{R}^{d_v}$ corresponds to the feature vector of the i-th sample from view v. The similarity matrix $\mathbf{S}^v$ is updated by keeping only the K-nearest neighbors; following this, the degree matrix $\mathbf{D}^v$ is given by $\mathrm{diag}(\sum_{j=1}^n \mathbf{S}^v_{ij})$. The normalized Laplacian matrix for view v is given by Eq. (27).

Update $\mathbf{L_s}$

$$\mathbf{L_s} = \mathbf{I} - \mathbf{D}^{-1/2}\mathbf{S}\mathbf{D}^{-1/2} \tag{28}$$

Following the construction in the main text, we compute the normalized shared Laplacian matrix $\mathbf{L_s}$ according to Eq. (28).

Impute $\mathbf{X}^v$

$$\mathbf{X}^v = \mathbf{A}^v\mathbf{Z}^v\mathbf{W}^v \tag{29}$$

This equation utilizes the indicator matrix $\mathbf{W}^v$ to reconstruct the columns in $\mathbf{X}^v$ that correspond to missing samples. Algorithm 1 provides a summary of the complete optimization process of GUITAR.

Algorithm 1 Optimization Algorithm of GUITAR

Input: Incomplete multi-view data$\{\mathbf{X}^1, \ldots, \mathbf{X}^m\}$, cluster number c, trade-off parameter $\lambda_1, \lambda_2, \lambda_3$ and anchor number t.
Output: Clustering results

Initialize: $\forall v, \mathbf{Z}^v = \mathbf{1}, \mathbf{E}^v = \mathbf{0}, \mathbf{Y}^v = \mathbf{0}, \boldsymbol{\mathcal{G}} = \mathbf{0}, \boldsymbol{\mathcal{Q}} = \mathbf{0}, \mu = 10^{-4}, \rho = 10^{-4}, \eta_\mu = \eta_\rho = 1.2, \mu_{\max} = \rho_{\max} = 10^{12}, \epsilon = 10^{-7}$
while not converge **do**
  Update $\{\mathbf{A}^v\}_{v=1}^m$ by Eq. (13)
  Update $\{\mathbf{E}^v\}_{v=1}^m$ by Eq. (15)
  Update $\{\boldsymbol{\Sigma}^v\}_{v=1}^m$ by Eq. (17)
  Update $\{\mathbf{Z}^v\}_{v=1}^m$ by Eq. (20)
  Update $\{\boldsymbol{\mathcal{G}}^v\}_{v=1}^m$ by Eq. (23)
  Update $\{\mathbf{Y}^v\}_{v=1}^m, \boldsymbol{\mathcal{Q}}, \mu, \rho$ by Eq. (26)
  Update $\{\mathbf{L}^v\}_{v=1}^m$ by Eq. (27)
  Update $\mathbf{L_s}$ by Eq. (28)
  Update $\{\mathbf{X}^v\}_{v=1}^m$ by Eq. (29)
  Check the convergence conditions: $\|\mathbf{X}^v - \mathbf{A}^v\mathbf{Z}^v - \mathbf{E}^v\|_\infty < \epsilon$ and $\|\mathbf{Z}^v - \boldsymbol{\mathcal{G}}^v\|_\infty < \epsilon$
end while
Output clustering results via performing k-means on the left singular vectors of $\frac{1}{\sqrt{m}}[(\mathbf{Z}^1)^\top, \ldots, (\mathbf{Z}^m)^\top]$.

A.5 Convergence proof

In this section, we present the convergence analysis of the proposed model. We begin by introducing a supporting lemma, and then proceed to prove Theorem 1 as stated in the main text.

Lemma 1 *[52]Assume a function $F : \mathbb{R}^{m\times n} \to \mathbb{R}$ is defined by the composition $F(\mathbf{X}) = f(\boldsymbol{\kappa}(\mathbf{X}))$, where $\boldsymbol{\kappa}(\mathbf{X}) = (\sigma_1(\mathbf{X}), \ldots, \sigma_r(\mathbf{X}))$ denotes the vector of singular values of $\mathbf{X} \in \mathbb{R}^{m\times n}$, with $r = \min(m, n)$. Let the singular value decomposition of $\mathbf{X}$ be $\mathbf{X} = \mathbf{U}\mathrm{diag}(\boldsymbol{\kappa}(\mathbf{X}))\mathbf{V}^\top$, and assume the function $f : \mathbb{R}^r \to \mathbb{R}$ is absolutely symmetric and differentiable at $\boldsymbol{\kappa}(\mathbf{X})$. Under these assumptions, the subdifferential of $F(\mathbf{X})$ at $\mathbf{X}$ is given by*

$$\frac{\partial F(\mathbf{X})}{\partial \mathbf{X}} = \mathbf{U}\mathrm{diag}(\partial f(\boldsymbol{\kappa}(\mathbf{X})))\mathbf{V}^\top \tag{30}$$

where $\partial f(\boldsymbol{\kappa}(\mathbf{X})) = \left(\frac{\partial f(\sigma_1(\mathbf{X}))}{\partial \mathbf{X}}, \ldots, \frac{\partial f(\sigma_r(\mathbf{X}))}{\partial \mathbf{X}}\right)$.

Proof of the boundedness of the sequence $\{\mathcal{J}_p\}_{p=1}^{\infty}$: At the $(p+1)$-th iteration, the column update for $\mathbf{E}_{p+1}^v$ is

$$\mathbf{e}_{q,p+1}^v = (\lambda_1(\Sigma^v)^{-1} + \mu_p I)^{-1}\Big[\mathbf{y}_{q,p}^v + \mu_p(\mathbf{x}_q^v - \mathbf{A}^v\mathbf{z}_{q,p+1}^v)\Big] \tag{31}$$

The multiplier update is

$$\mathbf{y}_{q,p+1}^v = \mathbf{y}_{q,p}^v + \mu_p(\mathbf{x}_q^v - \mathbf{A}^v\mathbf{z}_{q,p+1}^v - \mathbf{e}_{q,p+1}^v) \tag{32}$$

Substituting $\mathbf{e}_{q,p+1}^v$ into the multiplier update, we can factor terms to obtain

$$\mathbf{y}_{q,p+1}^v = \Big(I - \mu_p(\lambda_1(\Sigma^v)^{-1} + \mu_p I)^{-1}\Big)\mathbf{y}_{q,p}^v + \mu_p\Big(I + \mu_p(\lambda_1(\Sigma^v)^{-1} + \mu_p I)^{-1}\Big)(\mathbf{x}_q^v - \mathbf{A}^v\mathbf{z}_{q,p+1}^v) \tag{33}$$

Taking the ℓ_2-norm and using submultiplicativity yields

$$\|\mathbf{y}_{q,p+1}^v\|_2 \le \Upsilon_1\|\mathbf{y}_{q,p}^v\|_2 + \Upsilon_2\|\mathbf{x}_q^v - \mathbf{A}^v\mathbf{z}_{q,p+1}^v\|_2, \tag{34}$$

where $\Upsilon_1 = \|I - \mu_p(\lambda_1(\Sigma^v)^{-1} + \mu_p I)^{-1}\|_2$, $\quad \Upsilon_2 = \|\mu_p\Big(I + \mu_p(\lambda_1(\Sigma^v)^{-1} + \mu_p I)^{-1}\Big)\|_2$. Given that Σ^v is a positive definite covariance matrix and the regularization in Eq. 17, the inverse matrix $(\Sigma^v)^{-1}$ possesses a bounded spectral norm. With λ_1 constant and μ_p bounded, Υ_1 and Υ_2 are bounded constants. Finally, the initial multiplier $\mathbf{y}_{q,0}^v$ and the data term $\mathbf{x}_q^v - \mathbf{A}^v\mathbf{z}_{q,p+1}^v$ are bounded, the recursion implies $\sup_p \|\mathbf{y}_{q,p}^v\|_2 < \infty$ and therefore the sequence $\{\mathbf{Y}_p^v\}$ is bounded.

The first-order optimality condition with respect to $\boldsymbol{\mathcal{G}}_{p+1}$ at iteration $(p+1)$ yields:

$$\mathbf{0} = \partial\|\boldsymbol{\mathcal{G}}_{p+1}\|_{\mathrm{HP}\ell_\delta} + \rho_p(\boldsymbol{\mathcal{G}}_{p+1} - \boldsymbol{\mathcal{Z}}_{p+1}) - \boldsymbol{\mathcal{Q}}_p \tag{35}$$

In conjunction with the update rule:

$$\boldsymbol{\mathcal{Q}}_{p+1} = \boldsymbol{\mathcal{Q}}_p + \rho_p(\boldsymbol{\mathcal{Z}}_{p+1} - \boldsymbol{\mathcal{G}}_{p+1}) \tag{36}$$

we obtain the following relationship:

$$\partial\|\boldsymbol{\mathcal{G}}_{p+1}\|_{\mathrm{HP}\ell_\delta} = \boldsymbol{\mathcal{Q}}_{p+1} \tag{37}$$

The tensor $\boldsymbol{\mathcal{G}}$ admits a t-SVD decomposition of the form $\boldsymbol{\mathcal{G}} = \boldsymbol{\mathcal{U}} * \boldsymbol{\mathcal{S}} * \boldsymbol{\mathcal{V}}^\top$. By invoking Lemma 1, it follows that

$$\begin{aligned}\left\|\partial\left\|\boldsymbol{\mathcal{G}}_{p+1}\right\|_{\mathrm{HP}\ell_\delta}\right\|_F^2 &= \left\|\frac{1}{n_3}\boldsymbol{\mathcal{U}} * \mathrm{ifft}\left(\partial f\left(\boldsymbol{\mathcal{S}}_f\right), [], 3\right) * \boldsymbol{\mathcal{V}}^\top\right\|_F^2 \\ &= \frac{1}{n_3^3}\|\partial f(\boldsymbol{\mathcal{S}}_f)\|_F^2 \le \frac{1}{n_3^3}\sum_{k=1}^{n_3}\sum_{j=1}^{\min(n_1,n_2)}[\partial f(\boldsymbol{\mathcal{S}}_f^k(j,j))]^2\end{aligned} \tag{38}$$

Therefore, the Frobenius norm of the subgradient $\partial\left\|\boldsymbol{\mathcal{G}}_{p+1}\right\|_{\mathrm{HP}\ell_\delta}$ is upper-bounded by a finite quantity, indicating that it remains bounded. In light of Eq. (37), this further implies that the sequence $\{\boldsymbol{\mathcal{Q}}_p\}_{p=1}^{\infty}$ is also bounded.

Furthermore, based on the update rules described in **Algorithm 1**, we can derive the following inequality:

$$\begin{aligned}
&\mathcal{L}(\mathbf{A}_{p+1}^v, \mathbf{E}_{p+1}^v, \mathbf{Z}_{p+1}^v, \mathbf{\Sigma}_{p+1}^v, \boldsymbol{\mathcal{G}}_{p+1}, \mathbf{Y}_p^v, \boldsymbol{\mathcal{Q}}_p, \mu_p, \rho_p) \\
&\leq \mathcal{L}(\mathbf{A}_p^v, \mathbf{E}_p^v, \mathbf{Z}_p^v, \mathbf{\Sigma}_p^v, \boldsymbol{\mathcal{G}}_p, \mathbf{Y}_p^v, \boldsymbol{\mathcal{Q}}_p, \mu_p, \rho_p) \\
&= \mathcal{L}(\mathbf{A}_p^v, \mathbf{E}_p^v, \mathbf{Z}_p^v, \mathbf{\Sigma}_p^v, \boldsymbol{\mathcal{G}}_p, \mathbf{Y}_{p-1}^v, \boldsymbol{\mathcal{Q}}_{p-1}, \mu_{p-1}, \rho_{p-1}) \\
&\quad + \frac{\rho_p + \rho_{p-1}}{2\rho_{p-1}^2} \left\| \boldsymbol{\mathcal{Q}}_p - \boldsymbol{\mathcal{Q}}_{p-1} \right\|_F^2 \\
&\quad + \frac{\mu_p + \mu_{p-1}}{2\mu_{p-1}^2} \sum_{v=1}^{m} \left\| \mathbf{Y}_p^v - \mathbf{Y}_{p-1}^v \right\|_F^2
\end{aligned} \tag{39}$$

By recursively expanding the right-hand side of the inequality from $p = 1$ to n, we obtain:

$$\begin{aligned}
&\mathcal{L}(\mathbf{A}_{p+1}^v, \mathbf{E}_{p+1}^v, \mathbf{Z}_{p+1}^v, \mathbf{\Sigma}_{p+1}^v, \boldsymbol{\mathcal{G}}_{p+1}, \mathbf{Y}_p^v, \boldsymbol{\mathcal{Q}}_p, \mu_p, \rho_p) \\
&\leq \mathcal{L}(\mathbf{A}_1^v, \mathbf{E}_1^v, \mathbf{Z}_1^v, \mathbf{\Sigma}_1^v, \boldsymbol{\mathcal{G}}_1, \mathbf{Y}_0^v, \boldsymbol{\mathcal{Q}}_0, \mu_0, \rho_0) \\
&\quad + \sum_{p=1}^{n} \frac{\rho_p + \rho_{p-1}}{2\rho_{p-1}^2} \left\| \boldsymbol{\mathcal{Q}}_p - \boldsymbol{\mathcal{Q}}_{p-1} \right\|_F^2 \\
&\quad + \sum_{p=1}^{n} \left(\frac{\mu_p + \mu_{p-1}}{2\mu_{p-1}^2} \sum_{v=1}^{m} \left\| \mathbf{Y}_p^v - \mathbf{Y}_{p-1}^v \right\|_F^2 \right)
\end{aligned} \tag{40}$$

It is straightforward to verify that:

$$\sum_{p=1}^{n} \frac{\rho_p + \rho_{p-1}}{2\rho_{p-1}^2} < \infty, \quad \sum_{p=1}^{n} \frac{\mu_p + \mu_{p-1}}{2\mu_{p-1}^2} < \infty \tag{41}$$

Given that the initial objective value $\mathcal{L}(\mathbf{A}_1^v, \mathbf{E}_1^v, \mathbf{Z}_1^v, \mathbf{\Sigma}_1^v, \boldsymbol{\mathcal{G}}_1, \mathbf{Y}_0^v, \boldsymbol{\mathcal{Q}}_0, \mu_0, \rho_0)$ is finite, and the sequences $\{\mathbf{Y}_p^v\}_{p=1}^{\infty}$, $\{\boldsymbol{\mathcal{Q}}_p\}_{p=1}^{\infty}$, along with the summations $\sum_{p=1}^{n} \frac{\rho_p + \rho_{p-1}}{2\rho_{p-1}^2}$ and $\sum_{p=1}^{n} \frac{\mu_p + \mu_{p-1}}{2\mu_{p-1}^2}$ are all bounded, we conclude that the augmented Lagrangian $\mathcal{L}(\mathbf{A}_{p+1}^v, \mathbf{E}_{p+1}^v, \mathbf{Z}_{p+1}^v, \mathbf{\Sigma}_{p+1}^v, \boldsymbol{\mathcal{G}}_{p+1}, \mathbf{Y}_p^v, \boldsymbol{\mathcal{Q}}_p, \mu_p, \rho_p)$ remains bounded throughout the iterations.

Recalling the following equality:

$$\begin{aligned}
&\mathcal{L}(\mathbf{A}_{p+1}^v, \mathbf{E}_{p+1}^v, \mathbf{Z}_{p+1}^v, \mathbf{\Sigma}_{p+1}^v, \boldsymbol{\mathcal{G}}_{p+1}, \mathbf{Y}_p^v, \boldsymbol{\mathcal{Q}}_p, \mu_p, \rho_p) \\
&= \|\boldsymbol{\mathcal{G}}_{p+1}\|_{\mathrm{HP}\ell_\delta} - \lambda_1 \sum_{v=1}^{m} \left(\sum_{q=1}^{n} \ln\left(\mathcal{N}(\mathbf{e}_{q,p+1}^v \mid \mathbf{0}, \mathbf{\Sigma}_{p+1}^v) \right) \right) + \langle \boldsymbol{\mathcal{Q}}_p, \boldsymbol{\mathcal{Z}}_{p+1} - \boldsymbol{\mathcal{G}}_{p+1} \rangle \\
&\quad + \sum_{v=1}^{m} \left(\left\langle \mathbf{Y}_p^v, \mathbf{X}^v - \mathbf{A}_{p+1}^v \mathbf{Z}_{p+1}^v - \mathbf{E}_{p+1}^v \right\rangle + \frac{\mu_p}{2} \left\| \mathbf{X}^v - \mathbf{A}_{p+1}^v \mathbf{Z}_{p+1}^v - \mathbf{E}_{p+1}^v \right\|_F^2 \right) \\
&\quad + \frac{\rho_p}{2} \left\| \boldsymbol{\mathcal{Z}}_{p+1} - \boldsymbol{\mathcal{G}}_{p+1} \right\|_F^2 + \lambda_2 \sum_{v=1}^{m} \sum_{\substack{v'=1 \\ v' \neq v}}^{m} \mathrm{Tr}(\mathbf{Z}_{p+1}^v \mathbf{L}^{v'} (\mathbf{Z}_{p+1}^v)^\top) + \lambda_3 \sum_{v=1}^{m} \mathrm{Tr}(\mathbf{Z}_{p+1}^v \mathbf{L}_{\mathbf{s}} (\mathbf{Z}_{p+1}^v)^\top)
\end{aligned} \tag{42}$$

and each term on the right-hand side of Eq. (42) is finite. Among all the components, particular attention is given to the term $\|\boldsymbol{\mathcal{G}}_{p+1}\|_{\mathrm{HP}\ell_\delta}$, which, being bounded, implies the boundedness of the associated singular values $\boldsymbol{\mathcal{S}}_f^k(j, j)$. As a result, we obtain the following relation:

$$\left\| \boldsymbol{\mathcal{G}}_{p+1} \right\|_F^2 = \frac{1}{n_3} \left\| \boldsymbol{\mathcal{G}}_{f,p+1} \right\|_F^2 = \frac{1}{n_3} \sum_{k=1}^{n_3} \sum_{j=1}^{\min(n_1, n_2)} [\boldsymbol{\mathcal{S}}_f^k(j, j)]^2 \tag{43}$$

which further implies that the sequence $\{\boldsymbol{\mathcal{G}}_p\}_{p=1}^{\infty}$ is bounded.

Moreover, it is readily observed from the update steps that the sequences $\{\mathbf{A}_p^v\}_{p=1}^{\infty}$, $\{\mathbf{E}_p^v\}_{p=1}^{\infty}$, $\{\mathbf{Z}_p^v\}_{p=1}^{\infty}$, and $\{\mathbf{\Sigma}_p^v\}_{p=1}^{\infty}$ are also bounded. Therefore, we conclude that the entire sequence $\left\{ \mathcal{J}_p = \mathbf{A}_p^v, \mathbf{E}_p^v, \mathbf{Z}_p^v, \mathbf{\Sigma}_p^v, \mathbf{Y}_p^v, \boldsymbol{\mathcal{G}}_p, \boldsymbol{\mathcal{Q}}_p \right\}_{p=1}^{\infty}$ remains within a finite range.

Establishing that the accumulation points converge to stationary KKT points: By invoking the Weierstrass–Bolzano theorem [53], the bounded sequence $\{\mathcal{J}_p\}_{p=1}^{\infty}$ is guaranteed to possess at least one accumulation point, which we denote by $\mathcal{J}_*$. Accordingly, we have:

$$\lim_{p\to\infty}(\mathbf{A}_p^v, \mathbf{E}_p^v, \mathbf{Z}_p^v, \mathbf{\Sigma}_p^v, \mathbf{Y}_p^v, \boldsymbol{\mathcal{G}}_p, \boldsymbol{\mathcal{Q}}_p) = (\mathbf{A}_*^v, \mathbf{E}_*^v, \mathbf{Z}_*^v, \mathbf{\Sigma}_*^v, \mathbf{Y}_*^v, \boldsymbol{\mathcal{G}}_*, \boldsymbol{\mathcal{Q}}_*) \tag{44}$$

In light of Eq. (26), we observe the following relationships:

$$\mathbf{X}^v - \mathbf{A}_{p+1}^v\mathbf{Z}_{p+1}^v - \mathbf{E}_{p+1}^v = \frac{\mathbf{Y}_{p+1}^v - \mathbf{Y}_p^v}{\mu_p}, \boldsymbol{\mathcal{Z}}_{p+1} - \boldsymbol{\mathcal{G}}_{p+1} = \frac{\boldsymbol{\mathcal{Q}}_{p+1} - \boldsymbol{\mathcal{Q}}_p}{\rho_p} \tag{45}$$

Given that both sequences $\{\mathbf{Y}_p^v\}_{p=1}^{\infty}$ and $\{\boldsymbol{\mathcal{Q}}_p\}_{p=1}^{\infty}$ are bounded, we obtain the following constraints at the accumulation point:

$$\mathbf{X}^v - \mathbf{A}_*^v\mathbf{Z}_*^v - \mathbf{E}_*^v = \mathbf{0}, \boldsymbol{\mathcal{Z}}_* - \boldsymbol{\mathcal{G}}_* = \mathbf{0} \tag{46}$$

Furthermore, due to the fact that $\mathbf{E}_{p+1}^v$ and $\boldsymbol{\mathcal{G}}_{p+1}$ satisfy the first-order optimality conditions, it follows that:

$$\mathbf{Y}_*^v = \lambda_1\partial\|\mathbf{E}_*^v\|_{\text{GRN}}, \quad \boldsymbol{\mathcal{Q}}_* = \partial\|\boldsymbol{\mathcal{G}}_*\|_{\text{HP}\ell_\delta} \tag{47}$$

Hence, the accumulation point $\mathcal{J}_*$ satisfies all necessary conditions of stationarity and primal feasibility. We thus conclude that any accumulation point of the sequence $\{\mathcal{J}_p\}_{p=1}^{\infty}$ corresponds to a stationary point that fulfills the KKT conditions of the proposed optimization problem.

A.6 Additional experimental results

Only a subset of the experimental figures was presented in the main text. In this subsection, we provide the remaining figures to offer a more complete view of the experimental results. Figure 6, Figure 7 and Figure 8 illustrates the sensitivity analysis on the remaining datasets with respect to the balance parameter, the number of anchors, and the parameter δ in the HPℓ_δ regularization. Figure 9 shows the convergence behavior across the remaining datasets, while Table 4 presents the ablation study results on those datasets.

Table 4: Ablation results of the GUITAR model across the remaining datasets.

Components / Datasets			COIL20MV			Mfeat			Scene		
GRN	DMR-1	DMR-2	ACC	NMI	PUR	ACC	NMI	PUR	ACC	NMI	PUR
✓			38.47	52.33	42.36	29.90	21.67	30.25	26.19	13.47	29.02
	✓		5.07	1.38	6.32	12.80	0.82	13.10	15.29	0.26	15.51
		✓	5.07	1.38	6.32	10.05	0.45	10.45	15.29	0.26	15.51
✓	✓		70.76	80.86	73.33	81.85	71.43	81.85	58.11	39.34	58.11
✓		✓	70.28	76.64	70.90	81.20	70.63	81.20	42.45	29.31	44.23
	✓	✓	5.07	1.38	6.32	10.05	0.45	10.45	15.29	0.26	15.51
✓	✓	✓	**73.89**	**82.44**	**74.58**	**82.35**	**71.86**	**82.35**	**58.18**	**39.88**	**58.18**

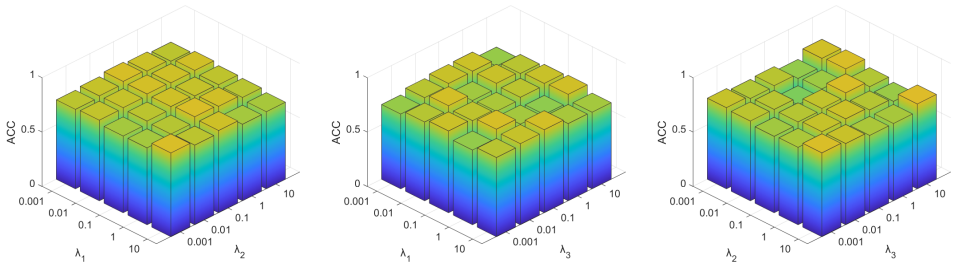

(a) COIL20MV

(b) COIL20MV

(c) COIL20MV

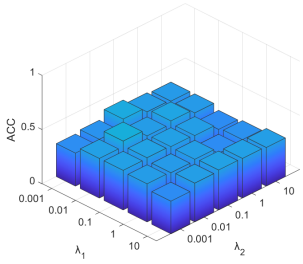

(d) EYaleB10

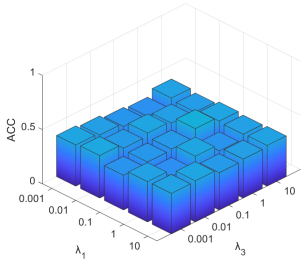

(e) EYaleB10

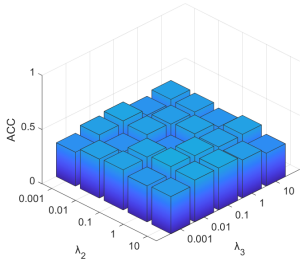

(f) EYaleB10

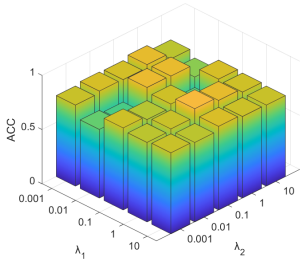

(g) MSRC_v1

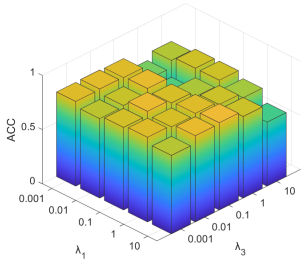

(h) MSRC_v1

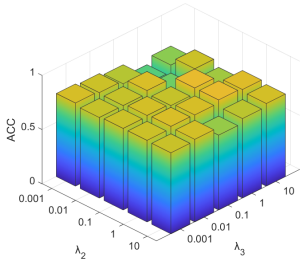

(i) MSRC_v1

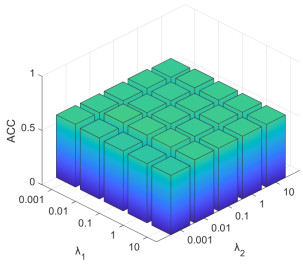

(j) Scene

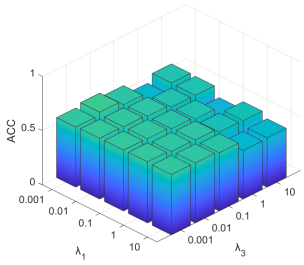

(k) Scene

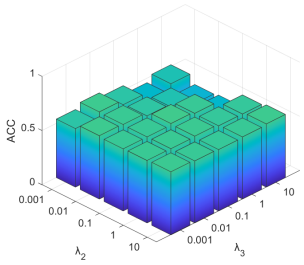

(l) Scene

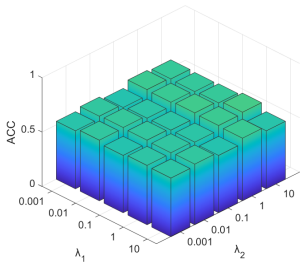

(m) Yale3

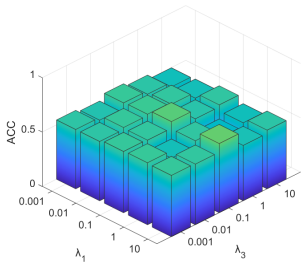

(n) Yale3

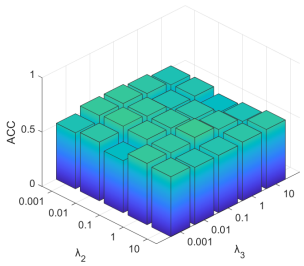

(o) Yale3

Figure 6: Sensitivity analysis of balancing parameters in the GUITAR model on the other datasets.

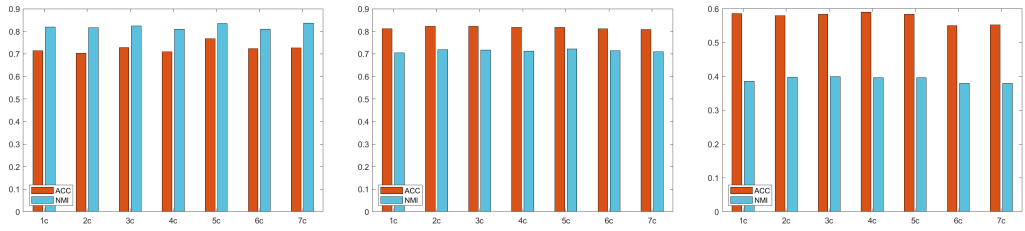

(a) COIL20MV (b) Mfeat (c) Scene

Figure 7: The impact of anchor count on the GUITAR model across the remaining datasets.

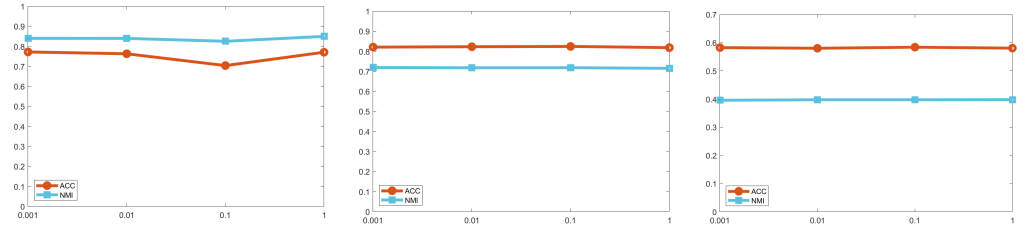

(a) COIL20MV (b) Mfeat (c) Scene

Figure 8: The impact of δ on the GUITAR model across the remaining datasets.

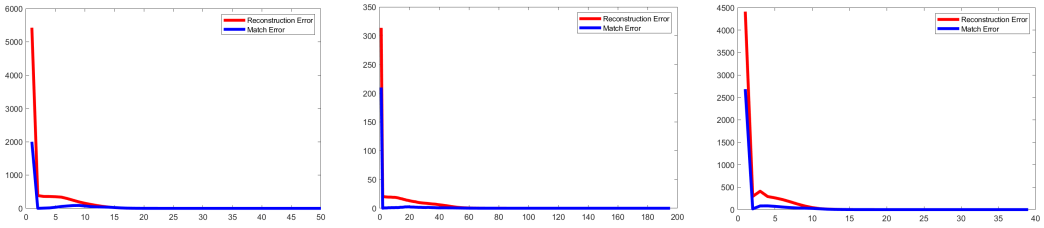

(a) Mfeat (b) MSRC_v1 (c) Scene

Figure 9: Convergence curves of the GUITAR model across the remaining datasets.

NeurIPS Paper Checklist

1. **Claims**

   Question: Do the main claims made in the abstract and introduction accurately reflect the paper's contributions and scope?

   Answer: [Yes]

   Justification: The abstract and introduction clearly and accurately summarize the paper's contributions and scope, which are consistent with the main claims presented throughout the paper.

   Guidelines:

   - The answer NA means that the abstract and introduction do not include the claims made in the paper.
   - The abstract and/or introduction should clearly state the claims made, including the contributions made in the paper and important assumptions and limitations. A No or NA answer to this question will not be perceived well by the reviewers.
   - The claims made should match theoretical and experimental results, and reflect how much the results can be expected to generalize to other settings.
   - It is fine to include aspirational goals as motivation as long as it is clear that these goals are not attained by the paper.

2. **Limitations**

   Question: Does the paper discuss the limitations of the work performed by the authors?

   Answer: [Yes]

   Justification: The paper explicitly discusses the computational complexity and hyperparameter sensitivity of the proposed method in the dedicated Limitations section.

   Guidelines:

   - The answer NA means that the paper has no limitation while the answer No means that the paper has limitations, but those are not discussed in the paper.
   - The authors are encouraged to create a separate "Limitations" section in their paper.
   - The paper should point out any strong assumptions and how robust the results are to violations of these assumptions (e.g., independence assumptions, noiseless settings, model well-specification, asymptotic approximations only holding locally). The authors should reflect on how these assumptions might be violated in practice and what the implications would be.
   - The authors should reflect on the scope of the claims made, e.g., if the approach was only tested on a few datasets or with a few runs. In general, empirical results often depend on implicit assumptions, which should be articulated.
   - The authors should reflect on the factors that influence the performance of the approach. For example, a facial recognition algorithm may perform poorly when image resolution is low or images are taken in low lighting. Or a speech-to-text system might not be used reliably to provide closed captions for online lectures because it fails to handle technical jargon.
   - The authors should discuss the computational efficiency of the proposed algorithms and how they scale with dataset size.
   - If applicable, the authors should discuss possible limitations of their approach to address problems of privacy and fairness.
   - While the authors might fear that complete honesty about limitations might be used by reviewers as grounds for rejection, a worse outcome might be that reviewers discover limitations that aren't acknowledged in the paper. The authors should use their best judgment and recognize that individual actions in favor of transparency play an important role in developing norms that preserve the integrity of the community. Reviewers will be specifically instructed to not penalize honesty concerning limitations.

3. **Theory assumptions and proofs**

   Question: For each theoretical result, does the paper provide the full set of assumptions and a complete (and correct) proof?

Answer: [Yes]

Justification: The paper provides a complete set of assumptions and a correct proof for each theoretical result discussed.

Guidelines:

- The answer NA means that the paper does not include theoretical results.
- All the theorems, formulas, and proofs in the paper should be numbered and cross-referenced.
- All assumptions should be clearly stated or referenced in the statement of any theorems.
- The proofs can either appear in the main paper or the supplemental material, but if they appear in the supplemental material, the authors are encouraged to provide a short proof sketch to provide intuition.
- Inversely, any informal proof provided in the core of the paper should be complemented by formal proofs provided in appendix or supplemental material.
- Theorems and Lemmas that the proof relies upon should be properly referenced.

4. **Experimental result reproducibility**

Question: Does the paper fully disclose all the information needed to reproduce the main experimental results of the paper to the extent that it affects the main claims and/or conclusions of the paper (regardless of whether the code and data are provided or not)?

Answer: [Yes]

Justification: The paper provides all the necessary details regarding the experimental setup, including model configurations, evaluation metrics, and data characteristics, ensuring that the main results can be reproduced even without the code or data.

Guidelines:

- The answer NA means that the paper does not include experiments.
- If the paper includes experiments, a No answer to this question will not be perceived well by the reviewers: Making the paper reproducible is important, regardless of whether the code and data are provided or not.
- If the contribution is a dataset and/or model, the authors should describe the steps taken to make their results reproducible or verifiable.
- Depending on the contribution, reproducibility can be accomplished in various ways. For example, if the contribution is a novel architecture, describing the architecture fully might suffice, or if the contribution is a specific model and empirical evaluation, it may be necessary to either make it possible for others to replicate the model with the same dataset, or provide access to the model. In general. releasing code and data is often one good way to accomplish this, but reproducibility can also be provided via detailed instructions for how to replicate the results, access to a hosted model (e.g., in the case of a large language model), releasing of a model checkpoint, or other means that are appropriate to the research performed.
- While NeurIPS does not require releasing code, the conference does require all submissions to provide some reasonable avenue for reproducibility, which may depend on the nature of the contribution. For example
  (a) If the contribution is primarily a new algorithm, the paper should make it clear how to reproduce that algorithm.
  (b) If the contribution is primarily a new model architecture, the paper should describe the architecture clearly and fully.
  (c) If the contribution is a new model (e.g., a large language model), then there should either be a way to access this model for reproducing the results or a way to reproduce the model (e.g., with an open-source dataset or instructions for how to construct the dataset).
  (d) We recognize that reproducibility may be tricky in some cases, in which case authors are welcome to describe the particular way they provide for reproducibility. In the case of closed-source models, it may be that access to the model is limited in some way (e.g., to registered users), but it should be possible for other researchers to have some path to reproducing or verifying the results.

5. **Open access to data and code**

   Question: Does the paper provide open access to the data and code, with sufficient instructions to faithfully reproduce the main experimental results, as described in supplemental material?

   Answer: [Yes]

   Justification: The paper provides open access to the data and code, with detailed instructions to faithfully reproduce the experimental results.

   Guidelines:

   - The answer NA means that paper does not include experiments requiring code.
   - Please see the NeurIPS code and data submission guidelines (`https://nips.cc/public/guides/CodeSubmissionPolicy`) for more details.
   - While we encourage the release of code and data, we understand that this might not be possible, so "No" is an acceptable answer. Papers cannot be rejected simply for not including code, unless this is central to the contribution (e.g., for a new open-source benchmark).
   - The instructions should contain the exact command and environment needed to run to reproduce the results. See the NeurIPS code and data submission guidelines (`https://nips.cc/public/guides/CodeSubmissionPolicy`) for more details.
   - The authors should provide instructions on data access and preparation, including how to access the raw data, preprocessed data, intermediate data, and generated data, etc.
   - The authors should provide scripts to reproduce all experimental results for the new proposed method and baselines. If only a subset of experiments are reproducible, they should state which ones are omitted from the script and why.
   - At submission time, to preserve anonymity, the authors should release anonymized versions (if applicable).
   - Providing as much information as possible in supplemental material (appended to the paper) is recommended, but including URLs to data and code is permitted.

6. **Experimental setting/details**

   Question: Does the paper specify all the training and test details (e.g., data splits, hyperparameters, how they were chosen, type of optimizer, etc.) necessary to understand the results?

   Answer: [Yes]

   Justification: Detailed experimental settings have been introduced in Section 4.

   Guidelines:

   - The answer NA means that the paper does not include experiments.
   - The experimental setting should be presented in the core of the paper to a level of detail that is necessary to appreciate the results and make sense of them.
   - The full details can be provided either with the code, in appendix, or as supplemental material.

7. **Experiment statistical significance**

   Question: Does the paper report error bars suitably and correctly defined or other appropriate information about the statistical significance of the experiments?

   Answer: [Yes]

   Justification: We present the standard deviation in Table 1.

   Guidelines:

   - The answer NA means that the paper does not include experiments.
   - The authors should answer "Yes" if the results are accompanied by error bars, confidence intervals, or statistical significance tests, at least for the experiments that support the main claims of the paper.
   - The factors of variability that the error bars are capturing should be clearly stated (for example, train/test split, initialization, random drawing of some parameter, or overall run with given experimental conditions).

- The method for calculating the error bars should be explained (closed form formula, call to a library function, bootstrap, etc.)
- The assumptions made should be given (e.g., Normally distributed errors).
- It should be clear whether the error bar is the standard deviation or the standard error of the mean.
- It is OK to report 1-sigma error bars, but one should state it. The authors should preferably report a 2-sigma error bar than state that they have a 96% CI, if the hypothesis of Normality of errors is not verified.
- For asymmetric distributions, the authors should be careful not to show in tables or figures symmetric error bars that would yield results that are out of range (e.g. negative error rates).
- If error bars are reported in tables or plots, The authors should explain in the text how they were calculated and reference the corresponding figures or tables in the text.

8. **Experiments compute resources**

   Question: For each experiment, does the paper provide sufficient information on the computer resources (type of compute workers, memory, time of execution) needed to reproduce the experiments?

   Answer: [Yes]

   Justification:We have provided detailed information about the computing resources in the experimental section.

   Guidelines:

   - The answer NA means that the paper does not include experiments.
   - The paper should indicate the type of compute workers CPU or GPU, internal cluster, or cloud provider, including relevant memory and storage.
   - The paper should provide the amount of compute required for each of the individual experimental runs as well as estimate the total compute.
   - The paper should disclose whether the full research project required more compute than the experiments reported in the paper (e.g., preliminary or failed experiments that didn't make it into the paper).

9. **Code of ethics**

   Question: Does the research conducted in the paper conform, in every respect, with the NeurIPS Code of Ethics `https://neurips.cc/public/EthicsGuidelines`?

   Answer: [Yes]

   Justification: The research conducted in the paper fully complies with the NeurIPS Code of Ethics.

   Guidelines:

   - The answer NA means that the authors have not reviewed the NeurIPS Code of Ethics.
   - If the authors answer No, they should explain the special circumstances that require a deviation from the Code of Ethics.
   - The authors should make sure to preserve anonymity (e.g., if there is a special consideration due to laws or regulations in their jurisdiction).

10. **Broader impacts**

    Question: Does the paper discuss both potential positive societal impacts and negative societal impacts of the work performed?

    Answer: [NA]

    Justification: The paper does not involve applications with direct societal implications.

    Guidelines:

    - The answer NA means that there is no societal impact of the work performed.
    - If the authors answer NA or No, they should explain why their work has no societal impact or why the paper does not address societal impact.

- Examples of negative societal impacts include potential malicious or unintended uses (e.g., disinformation, generating fake profiles, surveillance), fairness considerations (e.g., deployment of technologies that could make decisions that unfairly impact specific groups), privacy considerations, and security considerations.
- The conference expects that many papers will be foundational research and not tied to particular applications, let alone deployments. However, if there is a direct path to any negative applications, the authors should point it out. For example, it is legitimate to point out that an improvement in the quality of generative models could be used to generate deepfakes for disinformation. On the other hand, it is not needed to point out that a generic algorithm for optimizing neural networks could enable people to train models that generate Deepfakes faster.
- The authors should consider possible harms that could arise when the technology is being used as intended and functioning correctly, harms that could arise when the technology is being used as intended but gives incorrect results, and harms following from (intentional or unintentional) misuse of the technology.
- If there are negative societal impacts, the authors could also discuss possible mitigation strategies (e.g., gated release of models, providing defenses in addition to attacks, mechanisms for monitoring misuse, mechanisms to monitor how a system learns from feedback over time, improving the efficiency and accessibility of ML).

11. **Safeguards**

    Question: Does the paper describe safeguards that have been put in place for responsible release of data or models that have a high risk for misuse (e.g., pretrained language models, image generators, or scraped datasets)?

    Answer: [NA]

    Justification: The paper does not describe safeguards for the responsible release of data or models with a high risk of misuse.

    Guidelines:

    - The answer NA means that the paper poses no such risks.
    - Released models that have a high risk for misuse or dual-use should be released with necessary safeguards to allow for controlled use of the model, for example by requiring that users adhere to usage guidelines or restrictions to access the model or implementing safety filters.
    - Datasets that have been scraped from the Internet could pose safety risks. The authors should describe how they avoided releasing unsafe images.
    - We recognize that providing effective safeguards is challenging, and many papers do not require this, but we encourage authors to take this into account and make a best faith effort.

12. **Licenses for existing assets**

    Question: Are the creators or original owners of assets (e.g., code, data, models), used in the paper, properly credited and are the license and terms of use explicitly mentioned and properly respected?

    Answer: [Yes]

    Justification: The code for the comparison methods in the experimental section includes proper citations.

    Guidelines:

    - The answer NA means that the paper does not use existing assets.
    - The authors should cite the original paper that produced the code package or dataset.
    - The authors should state which version of the asset is used and, if possible, include a URL.
    - The name of the license (e.g., CC-BY 4.0) should be included for each asset.
    - For scraped data from a particular source (e.g., website), the copyright and terms of service of that source should be provided.

- If assets are released, the license, copyright information, and terms of use in the package should be provided. For popular datasets, `paperswithcode.com/datasets` has curated licenses for some datasets. Their licensing guide can help determine the license of a dataset.
- For existing datasets that are re-packaged, both the original license and the license of the derived asset (if it has changed) should be provided.
- If this information is not available online, the authors are encouraged to reach out to the asset's creators.

13. **New assets**

    Question: Are new assets introduced in the paper well documented and is the documentation provided alongside the assets?

    Answer: [Yes]

    Justification: We have provided the source code of our algorithm, which is included in the supplementary materials.

    Guidelines:

    - The answer NA means that the paper does not release new assets.
    - Researchers should communicate the details of the dataset/code/model as part of their submissions via structured templates. This includes details about training, license, limitations, etc.
    - The paper should discuss whether and how consent was obtained from people whose asset is used.
    - At submission time, remember to anonymize your assets (if applicable). You can either create an anonymized URL or include an anonymized zip file.

14. **Crowdsourcing and research with human subjects**

    Question: For crowdsourcing experiments and research with human subjects, does the paper include the full text of instructions given to participants and screenshots, if applicable, as well as details about compensation (if any)?

    Answer: [NA]

    Justification: The paper focuses on machine learning algorithm research and does not involve crowdsourcing or research with human subjects at all.

    Guidelines:

    - The answer NA means that the paper does not involve crowdsourcing nor research with human subjects.
    - Including this information in the supplemental material is fine, but if the main contribution of the paper involves human subjects, then as much detail as possible should be included in the main paper.
    - According to the NeurIPS Code of Ethics, workers involved in data collection, curation, or other labor should be paid at least the minimum wage in the country of the data collector.

15. **Institutional review board (IRB) approvals or equivalent for research with human subjects**

    Question: Does the paper describe potential risks incurred by study participants, whether such risks were disclosed to the subjects, and whether Institutional Review Board (IRB) approvals (or an equivalent approval/review based on the requirements of your country or institution) were obtained?

    Answer: [NA]

    Justification: Our manuscript focuses on algorithmic research and does not involve crowdsourcing or research with human subjects.

    Guidelines:

    - The answer NA means that the paper does not involve crowdsourcing nor research with human subjects.

- Depending on the country in which research is conducted, IRB approval (or equivalent) may be required for any human subjects research. If you obtained IRB approval, you should clearly state this in the paper.
- We recognize that the procedures for this may vary significantly between institutions and locations, and we expect authors to adhere to the NeurIPS Code of Ethics and the guidelines for their institution.
- For initial submissions, do not include any information that would break anonymity (if applicable), such as the institution conducting the review.

16. **Declaration of LLM usage**

    Question: Does the paper describe the usage of LLMs if it is an important, original, or non-standard component of the core methods in this research? Note that if the LLM is used only for writing, editing, or formatting purposes and does not impact the core methodology, scientific rigorousness, or originality of the research, declaration is not required.

    Answer: [NA]

    Justification: The core method development in this research does not involve large language models (LLMs) as any important, original, or non-standard components.

    Guidelines:

    - The answer NA means that the core method development in this research does not involve LLMs as any important, original, or non-standard components.
    - Please refer to our LLM policy (`https://neurips.cc/Conferences/2025/LLM`) for what should or should not be described.